GL02404

# Seismicity Report on the DIXIE VALLEY PROSPECT Churchill County, Nevada

## ABSTRACT

For twenty days in October and November of 1976, 200 square kilometers north of the Dixie Hot Springs in Central Nevada were surveyed for microearthquakes by use of a high gain (1-6M), high frequency (5-30Hz passband) seismic network. 216 events were detected in the immediate area. Fault-plane solutions indicate that the faulting in this area is an extrapolation of the tectonic style found in the major fault zones to the south. Conclusions are that fault intersections occur on the prospect, and, while their seismicity rate is not exceptional, the prospect is seismologically favorable for the occurrence of a geothermal reservoir. Confirmation of a heat source and a favorable hydrologic regime by electrical resistivity surveys is recommended. Caution should be observed because of recognized seismic risk in this area.

TABLE OF CONTENTS

FIGURES AND TABLES

# INTRODUCTION

A microearthquake survey to aid in the evaluation of the geothermal potential of the Dixie Valley prospect, Churchill County, Nevada, was conducted by MicroGeophysics (MGC) for twenty days in October, 1976. The prospect is near the Humbolt Salt Marsh and the Dixie Hot Springs (see the location and index map, Figure 1) in west central Nevada.

A high gain (1-6M at 20hz) high frequency (5-30 hz passband) seismic network (see instrument appendix) of 7 to 10 stations was deployed to survey the surrounding 200 $km^2$ for discrete, natural seismic events (microearthquakes) and thereby map tectonically active structures. The existence of recurrent, active tectonic processes is thought to be a necessary, but not sufficient, condition for the occurrence of commercial geothermal energy (Lange and Westphal, 1969; Ward and Bjornson, 1971; Ward and Jacob, 1971; Hamilton and Muffler, 1972; Ward, 1972). Although debate concerning acceptable geologic models for a geothermal system is continuing, an active tectonic system and the associated fracture porosity and permeability is an attractive target for geothermal exploration efforts. However, a seismically active system does not guarantee a heat source or the sufficient ground water supply necessary for a geothermal occurrence.

Sections of this report and their contents are listed below. The next section is a brief geological summary which includes a summary of the historical seismicity. Next is the operations summary which includes the survey parameters such as the magnitude detection threshold, the error prediction analysis, the velocity model, and the individual station parameters. The section on results contains the factual data obtained from the survey. Interpretation of these results is followed by the final sections which are the summary conclusions and recommendations of this report.

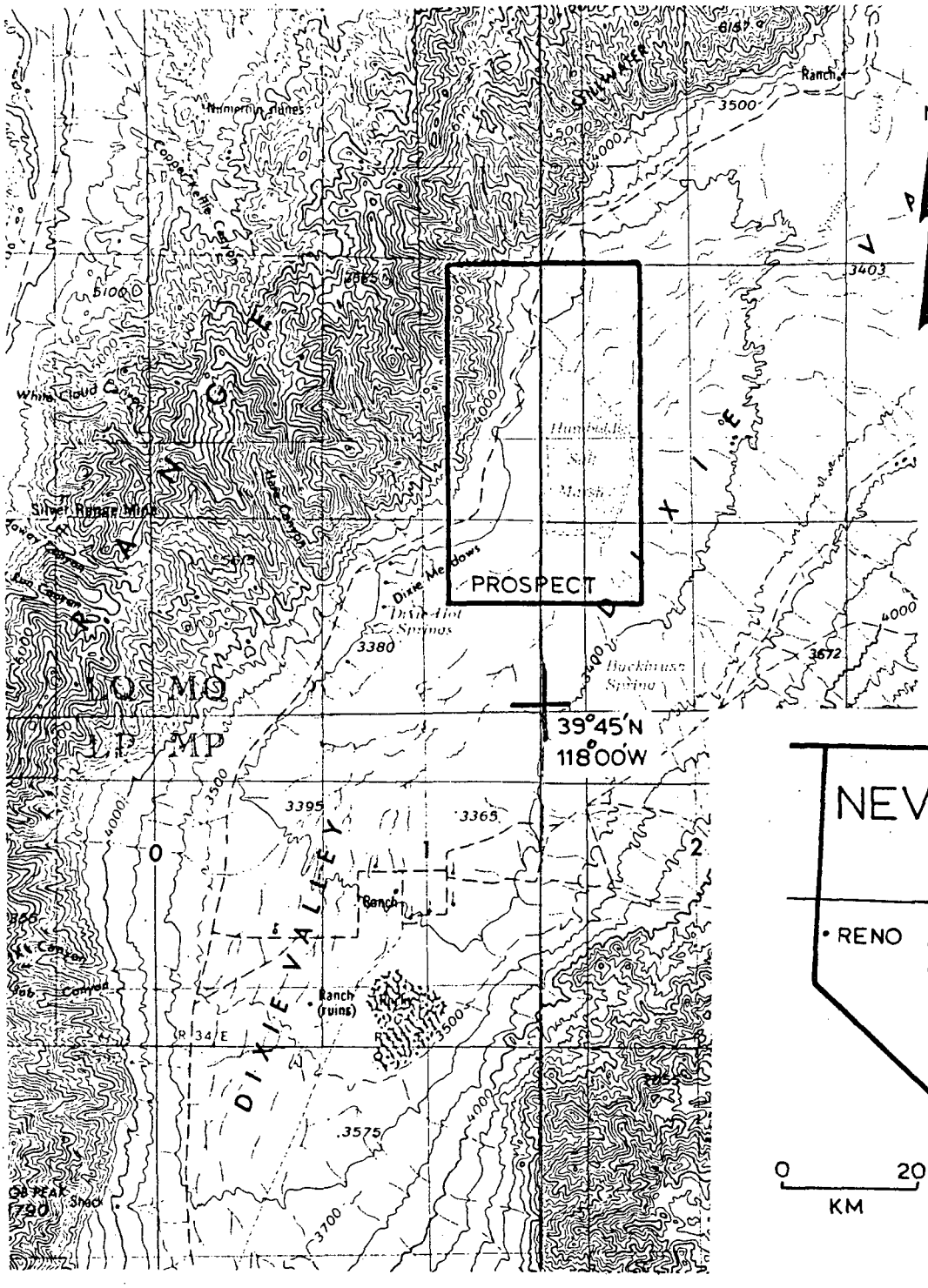


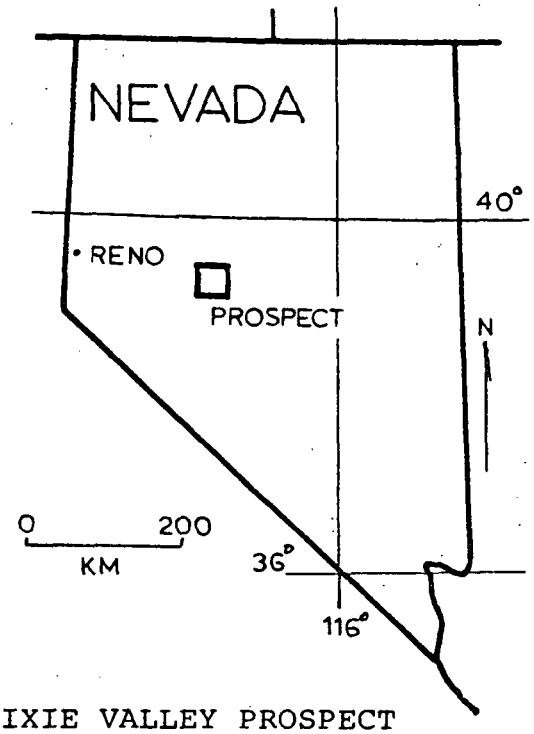


DIXIE VALLEY PROSPECT
CHURCHILL COUNTY, NEVADA

TITLE: LOCATION AND INDEX MAP

| | | |
|---|---|---|
| SCALE: N/A | APPROVED BY: JRB | DRAWN BY PB |
| DATE: DEC 13, 1975 | | REVISED N/A |
| Micro Geophysics | | Figure 1 |

## GEOLOGICAL AND GEOPHYSICAL BACKGROUND

The Dixie Valley prospect lies in the Basin and Range province. The area is characterized by north to north-northeast trending ranges separated by narrow valleys. Dixie Valley lies between the Stillwater mountains on the west and the Clan Alpine mountains on the east.

The following is a brief summary of the lithology of the major rock units in the prospect area followed by a brief description of the tectonics in the area. A schematic of the geology is shown in Figure 2.

Triassic metasediments and Upper Jurassic and Tertiary intrusives, volcanics and metavolcanics are exposed in the prospect area. Upper Triassic slate and phyllite is found at the southern end of the survey area. The Upper Jurassic Humboldt Gabbroic Complex is exposed in the eastern portion of the Stillwater range. This unit consists of shallowly emplaced gabbro and diorite that apparently broke the surface occasionally during intrusion forming an extrusive sequence of basalt flows, tuffs and breccias (Meister, 1967). Scattered early Tertiary plutons and diverse volcanics are also found in the Stillwaters. Capping the range and covering much of this area are 1800-4000' of Miocene volcanics including tuffs, breccias and a wide compositional range of flows. Dixie Valley is covered by unconsolidated lake and stream sediments of Plio-Pleisocene to recent age.

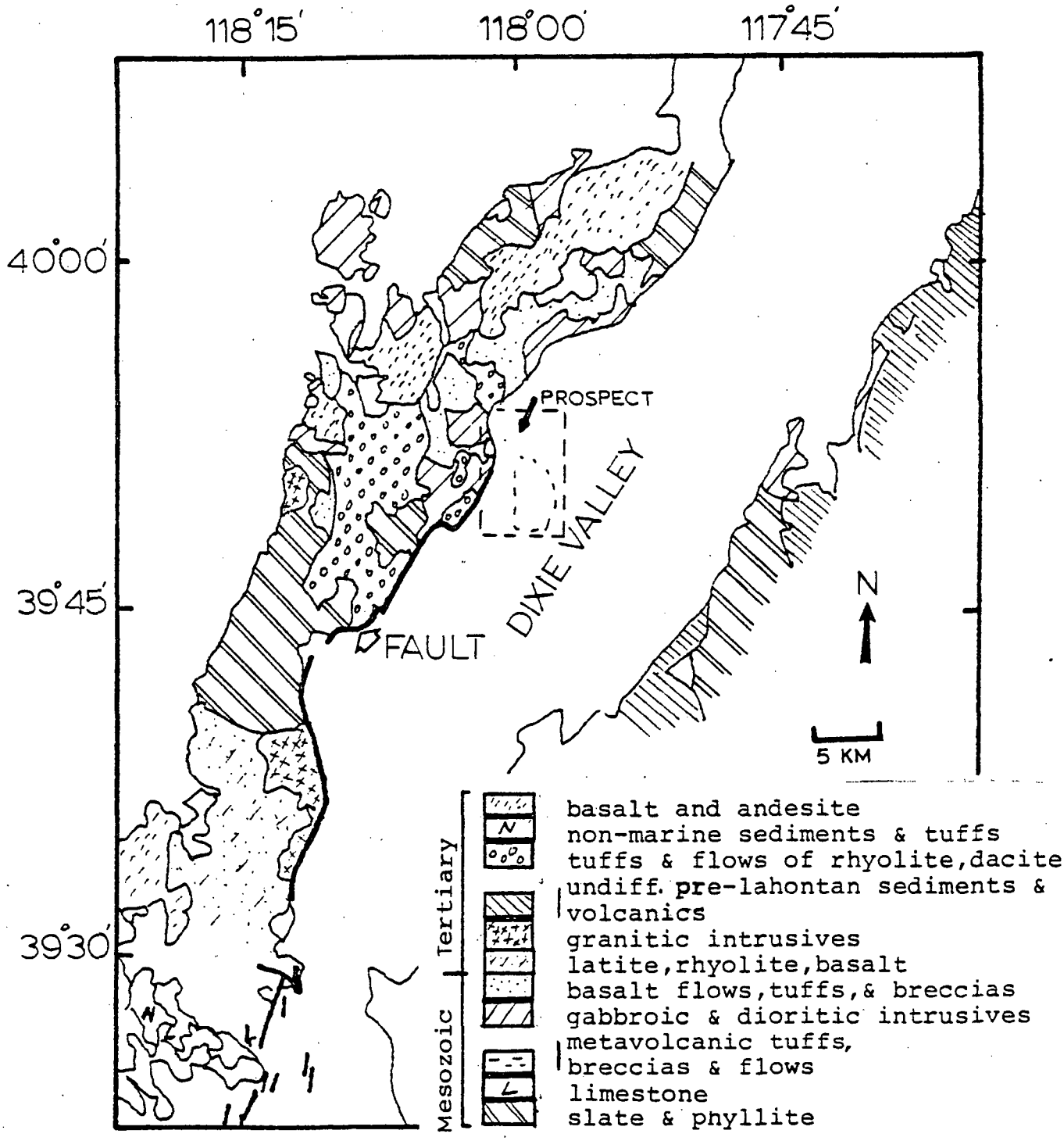


(AFTER MEISTER, 1967)

| | | |
|---|---|---|
| TITLE: GEOLOGIC MAP | | |
| SCALE: N/A | APPROVED BY: JRB | DRAWN BY PB |
| DATE: DEC 14, 1975 | | REVISED N/A |
| Micro Geophysics | | DRAWING NUMBER Figure 2 |

These include fan detritus, stream channel deposits and lacustrine sediments of primarily silt and clay.

Several major thrust faults are evident in the Stillwater Range. Triassic slates are underlain by a brecciated fault zone. In the north the slate rests disconcordantly on quartzite which overrides Jurassic metavolcanics which in turn overrides an undated limestone. Thus, to the north an imbricate-thrust zone is present. Elsewhere, gabbro of the Humboldt Gabbroic Complex overrides Triassic slate. It has been suggested that the shallow intrusion of the Humboldt Complex caused the motion of the thrust sheet. The suggested motion implies a late Jurassic age for the thrusting.

Cenezoic normal faulting has uplifted the Stillwater Range as a horst of narrow, north-trending blocks typical of Basin and Range structure. The attitude of basalt flows in the blocks evidences tilting of up to 12°. In some cases interior normal faults extend to the range margin, becoming part of the boundary fault. Often a series of step faults comprise the boundary fault with as many as four normal faults contributing to the structural relief between the range and valley (Herring, 1967).

The Dixie Valley fault has been active in historic time (Figure 2). Movement on this fault occurred at the time of the December 16, 1954 earthquake (Romney, 1957).

Displacement observed on surface faults was predominantly dip-slip in the Dixie Valley while it became diagonal-slip and strike-slip in the southern part of the fault system (Slemmings, 1957).

The historical seismicity and its relation to the geology will be discussed next. Dixie Valley is in the Nevada Seismic Zone and contains the northern end of a linear zone of concentrated seismic activity extending north from the Fairview Range. The source of this activity is the boundary fault between the Fairview Range and the Bell Flat grabben, the continuation of the boundary fault to the north, and the Dixie Valley Fault (Westphal and Lange, 1967). Movements on these faults were the source of energy for the 1954 earthquakes of magnitudes exceeding 6. Figure 3 is a plot of epicenters showing the seismic activity for two years, 1970 and 1971. The north-south trending pattern labeled A is the Fairview Peak-Dixie Valley seismic zone. Historically no earthquakes

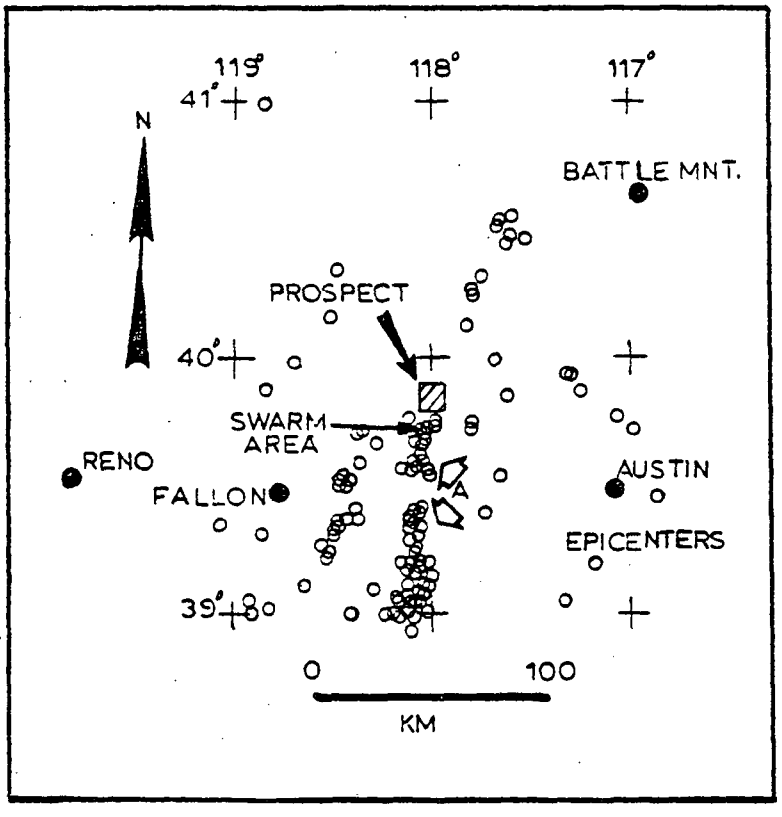


Figure 3. Historical Seismicity (after Nevada Bureau of Mines)

have occurred in the prospect area. The historical seismic activity is truncated just south of the prospect near Dixie Hot Springs, with a very active swarm center near the Dixie Hot Springs (Figure 3).

According to Gumper and Scholz (1971), the movement on the Dixie Valley fault is dip slip with minimal strike-slip. From observing the vertical displacement of the surface faulting, they excluded the possibility of a significant horizontal component. However, it appears that more than a single fault plane is needed as a mechanism to explain the observed seismicity of this fault system. At the southern extreme of the Fairview Peak fault, microearthquake hypocenters are concentrated at 10-15 km depth and are near the end of the surface faulting associated with the 1954 earthquakes (Stauder and Ryal, 1967). The hypocenters define two planar zones, one striking N 10° W and dipping 62° E, the other N 50° E, 50° SE. The former conforms with the trend of the whole Dixie Valley-Fairview Peak fault system. Surface faulting is terminated at the intersection of the two planes suggesting that the latter plane is a cross fault truncating the main system.

More recent microearthquake work in the Fairview Peak area has led to a more detailed model of the fault mechanism (Douglas and Ryall, 1972; Ryall and Mallone, 1971). They propose a zig-zag fault system consisting of northeast

trending tensional cracks and north-northwest trending compressional fractures (Figure 4). Motion on the Dixie Valley fault yields a fairly well-determined solution of right lateral oblique slip on a northeast trending fault plane.

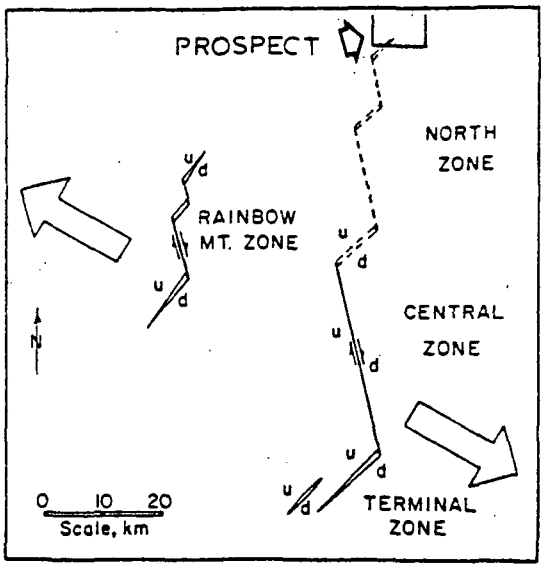


Figure 4. Fault Model (after Ryall and Malone, 1971)

## OPERATION SUMMARY

Ten seismic stations were used in the course of this survey. The technical description of the instruments is included in an appendix to this report.

Most stations were located on hard rock outcrops, except where array-geometry considerations dictated otherwise. Hardrock outcrop stations are superior to alluvial stations in both signal quality and the amount of ambient background noise. The increase in ambient background noise from an alluvial station to a nearby hard-rock station can often be 20 db. Therefore the signal-to-noise ratio of a network is improved if the majority of stations are placed on hard rock. Stations not placed on hard rock included stations 12, 13, 14, 15, 16, 17, and 18. At any one time during the survey no more than two of these stations were occupied.

Station locations were changed to maximize instrument gain and azimuthal coverage of the project area. All stations were operated at the gain limit allowed by the ambient background noise level. Table 1 is a detailed operational summary for the twenty day period of this survey. Coordinates of the seismograph stations are listed in Table 2 and displayed on Figure 5.

A detection threshold map (Figure 6) shows that the

 

# TABLE 1 OPERATION SCHEDULE

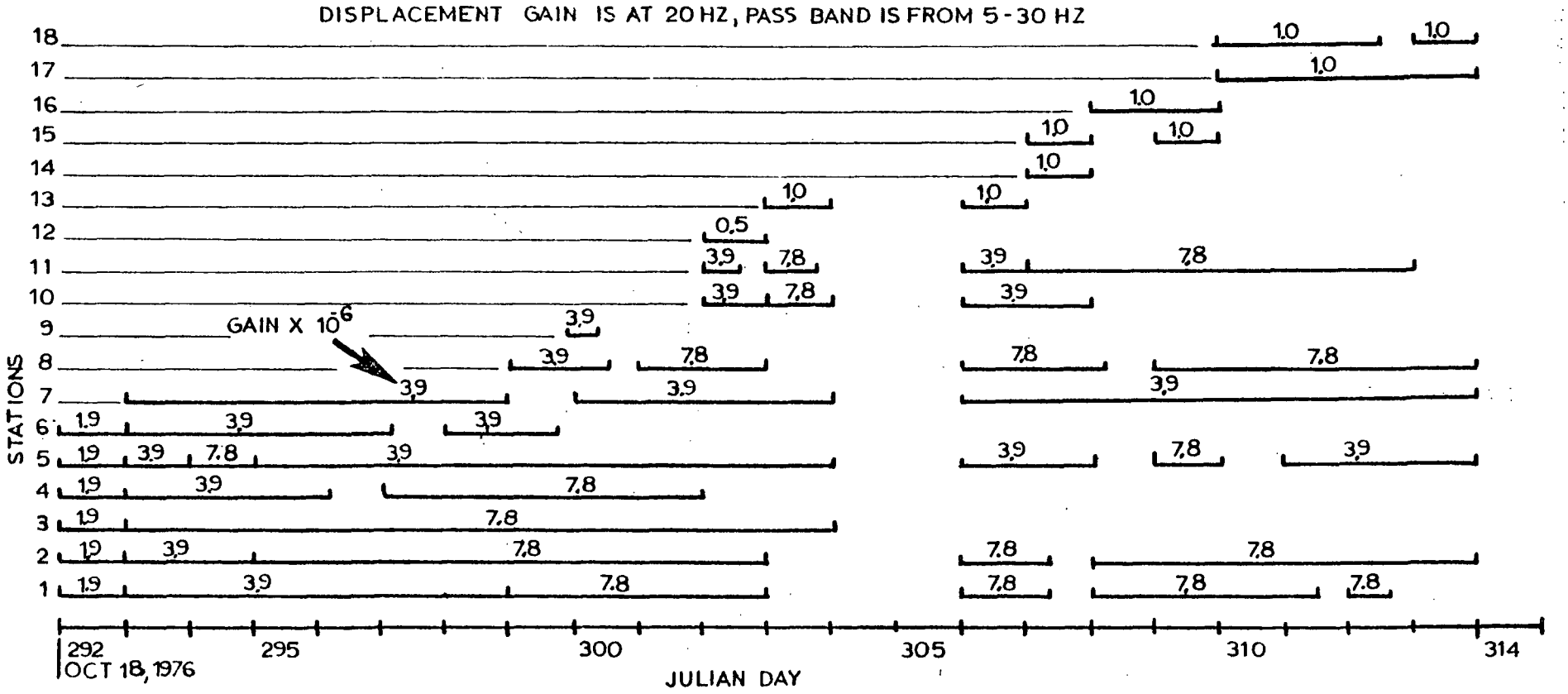

Table 2.

DIXIE VALLEY STATION COORDINATES

| Station | X (km) | Y (km) | Z (km) |
|---|---|---|---|
| 1 | 13.2 | 32.1 | 1.16 |
| 2 | 11.1 | 35.7 | 1.41 |
| 3 | 19.8 | 45.0 | 1.24 |
| 4 | 18.8 | 43.5 | 1.33 |
| 5 | 19.8 | 39.1 | 1.15 |
| 6 | 17.0 | 36.6 | 1.21 |
| 7 | 21.1 | 36.2 | 1.14 |
| 8 | 16.3 | 37.3 | 1.27 |
| 9 | 17.5 | 43.8 | 1.58 |
| 10 | 15.3 | 45.4 | 2.15 |
| 11 | 16.7 | 40.7 | 2.05 |
| 12 | 21.4 | 43.2 | 1.06 |
| 13 | 21.8 | 44.8 | 1.06 |
| 14 | 20.8 | 42.1 | 1.06 |
| 15 | 20.6 | 44.0 | 1.12 |
| 16 | 21.1 | 41.1 | 1.04 |
| 17 | 22.8 | 43.3 | 1.03 |
| 18 | 20.6 | 40.3 | 1.03 |

The origin is located at latitude 39°30' N, longitude 118°15'W. Z is the station altitude above sea level. Positive X and Y are east and north respectively. The accuracy of the coordinates are ± 0.10 km in X and Y and ± 0.02 km in Z.

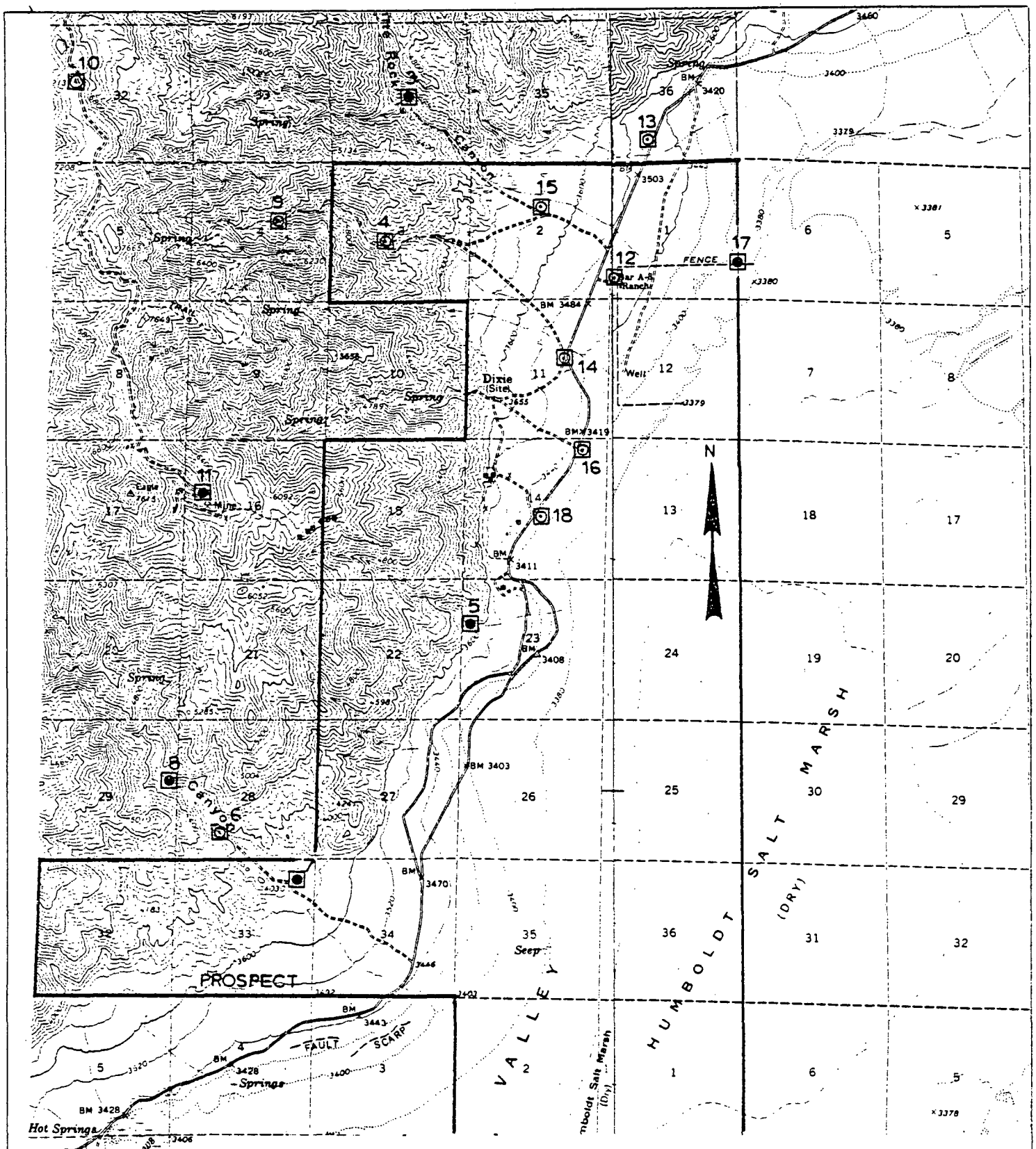


TITLE: STATION LOCATION MAP

| | | |
|---|---|---|
| SCALE: N/A | APPROVED BY: JRB | DRAWN BY PB |
| DATE: DEC 16, 1976 | | REVISED N/A |
| Micro Geophysics | | DRAWING NUMBER Figure 5 |

prospect area was surveyed for microearthquakes of magnitude -1.5 and larger. The line labeled "Mag.=-1" on Figure 6 is the surface projection of the volume within which a -1.0 magnitude earthquake would give at least a 2mm peak-to-peak displacement on at least one of the network stations. The analysis assumes normal attenuation as described by Brune and Allen (1967).

To further evaluate the seismic network, the technique of error prediction analysis (Peters and Crosson, 1972) was used to contour the expected precision of two of the station configurations. This technique requires an estimate of the uncertainties of the arrival times, velocity, and origin-time. Figures 7 and 8 show the estimates used and contours of the standard deviation of location parameters produced by the listed uncertainties. Thus the uncertainty of locations is generally $\pm$ 1.0 km in plan and $\pm$ 2.0 km in depth throughout the area of interest. The depth error increases rapidly away from the stations.

The velocity model is derived from previous work and from recordings of local events. Events were regarded as seismic in origin if they appeared on two or more stations with time difference corresponding to expected seismic velocities or if they had a signature similar to other larger events which could be traced across the network. Events were considered

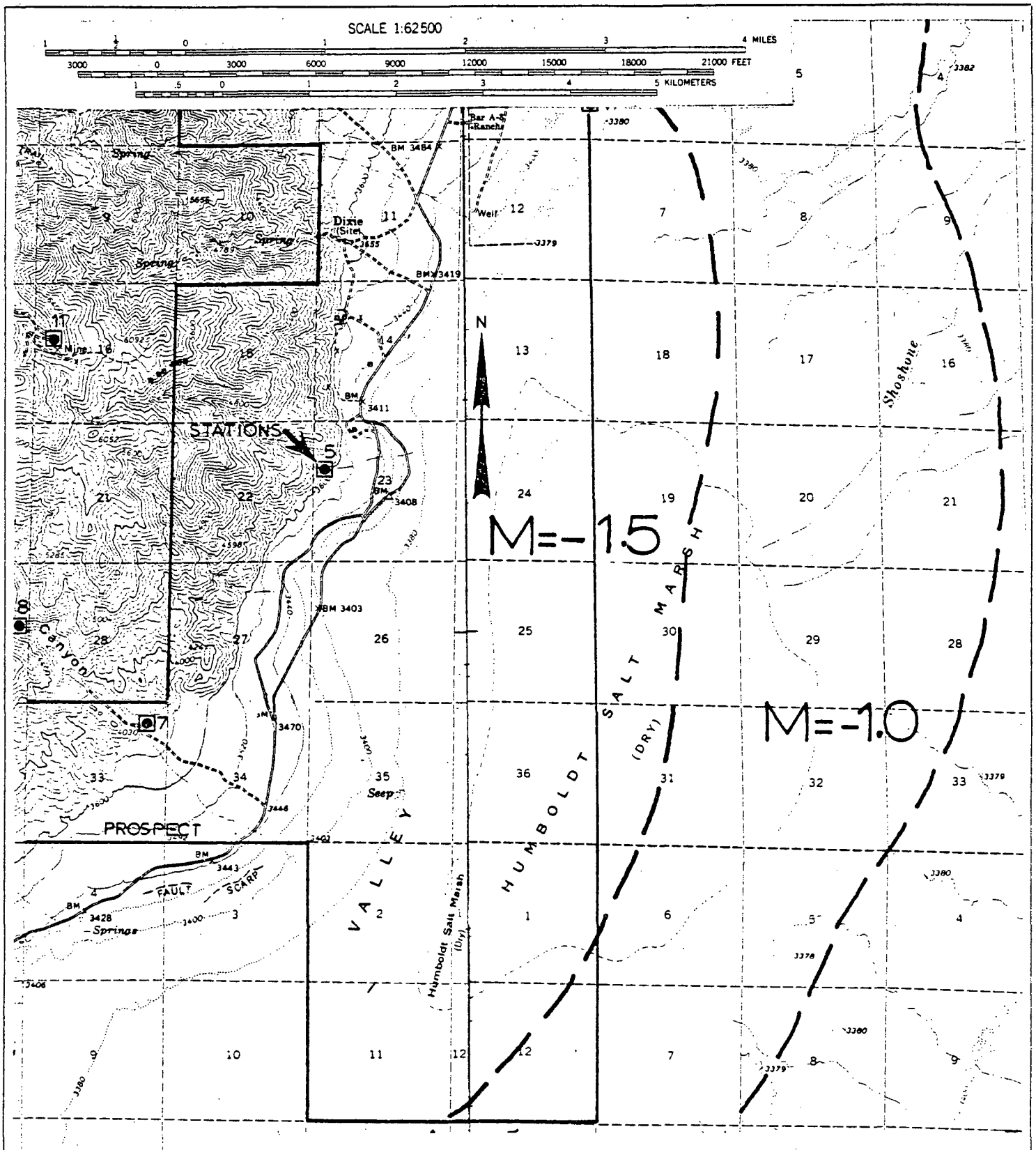


TITLE: DETECTION THRESHOLD MAP

| | | |
|---|---|---|
| SCALE: N/A | APPROVED BY: | DRAWN BY PB |
| DATE: DEC 16, 1976 | JRB | REVISED N/A |
| Micro Geophysics | | DRAWING NUMBER Figure 6 |

PREDICTED UNCERTAINTIES FOR X

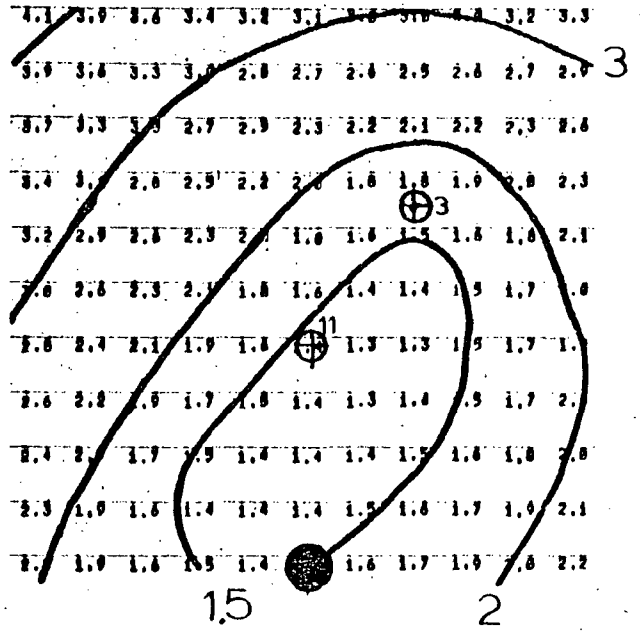


PREDICTED UNCERTAINTIES FOR Z

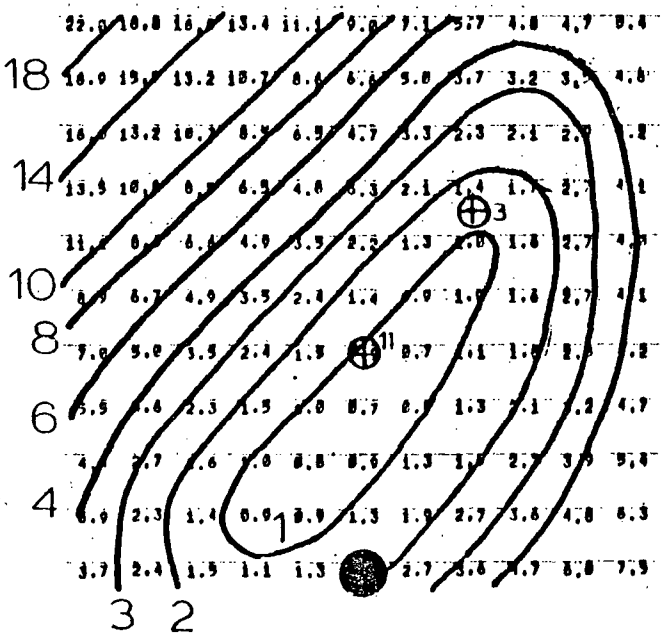


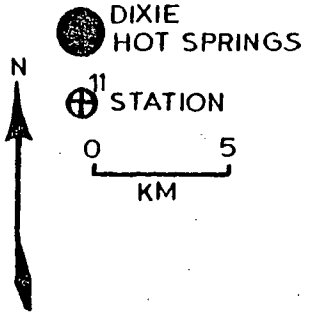


PREDICTED UNCERTAINTIES FOR Y

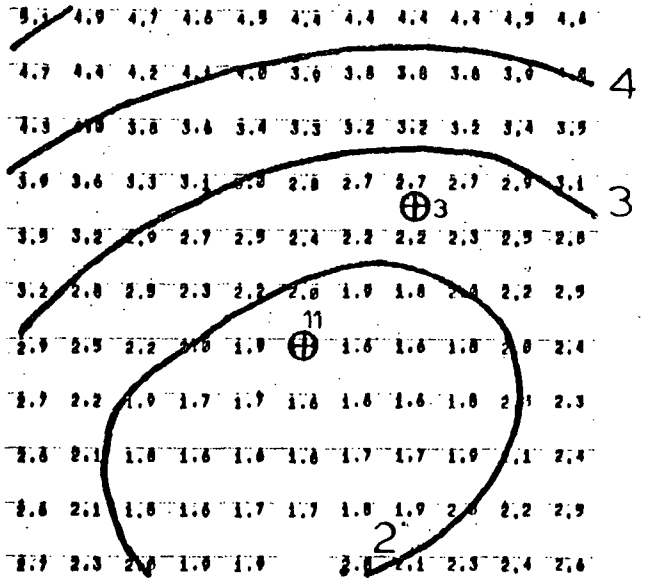


DIXIE VALLEY PROSPECT

AREA: $6 \leq X \leq 26$ KM
$32 \leq Y \leq 52$ KM

CONTOUR INTERVAL:
KM

HYPOCENTRAL DEPTH:
4 KM

VELOCITY MODEL:
HALF SPACE 4.5 KM/SEC

UNCERTAINTIES
TIME: + 30ms
VEL: 0.1 KM/sEC
ORIGIN
TIME: 0.300 SEC

| | | |
|---|---|---|
| TITLE: PREDICTED UNCERTAINTIES, AREA1 | | |
| SCALE: N/A | APPROVED BY: JRB | DRAWN BY PB |
| DATE: DEC 16,1976 | | REVISED N/A |
| Micro Geophysics | | DRAWING NUMBER Figure 7 |

(17)

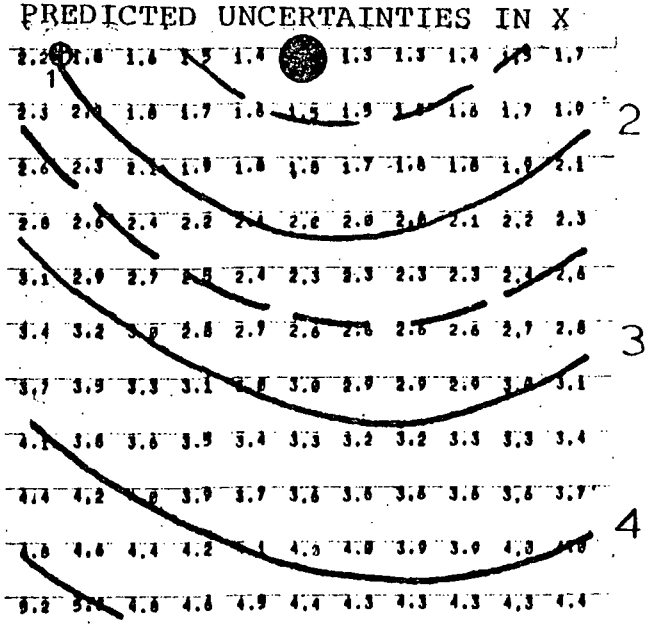


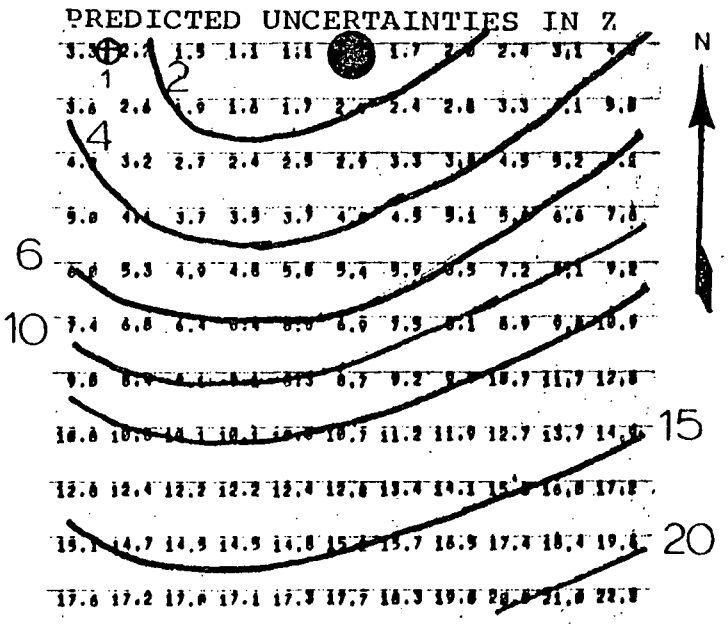


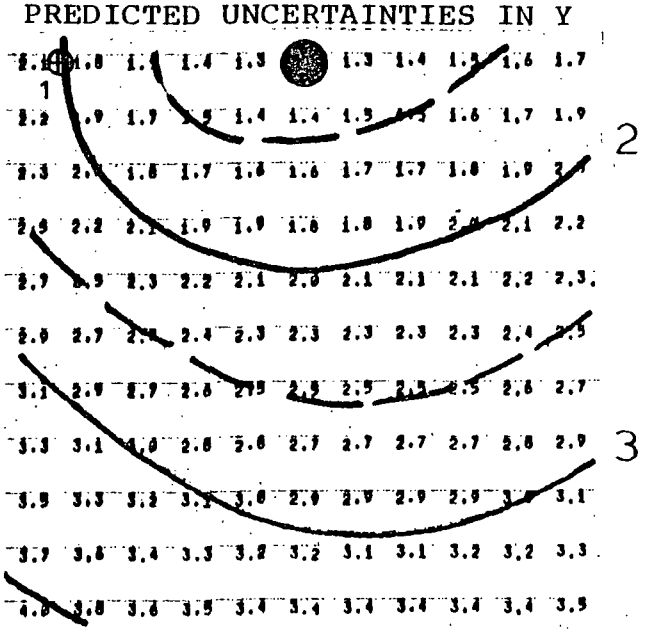


DIXIE VALLEY PROSPECT

AREA: $6 \leq X \leq 26$ KM
$12 \leq Y \leq 32$ KM

CONTOUR INTERVAL: KM

HYPOCENTRAL DEPTH 4 KM

VELOCITY MODEL: HALF SPACE 4.5 KM/SEC

UNCERTAINTIES
TIME: +30 ms
VEL: $\overline{0}$.1 KM/SEC

ORIGIN
TIME: 0.300 SEC

| | | |
|---|---|---|
| TITLE: PREDICTED UNCERTAINTIES, AREA 2 | | |
| SCALE: N/A | APPROVED BY: JRB | DRAWN BY PB |
| DATE: DEC 16, 1976 | | REVISED N/A |
| Micro Geophysics | | DRAWING NUMBER Figure 8 |

local if they had an S-P time of less than three seconds. Regional events and teleseisms were identified by signature and by S-P time. Regional events and teleseisms were considered outside the scope of this survey and therefore, no further analysis was performed on them.

Local events, timed on four or more stations, were located using a generalized-inverse computer program. This program, given a velocity model, least-square fits the calculated travel times to the observed arrival times. Events were read to $\pm$0.01 seconds for P arrivals and $\pm$0.1 seconds for S-p times. Amplitudes, peak to peak, were read to the nearest millimeter and the direction of the first motion when distinguishable, was noted.

The most critical parameter in the location procedure is the selection of an appropriate velocity model. The first step in this analysis was to run the observations through the location program assuming a constant velocity model, where $V_C$=4.0 Km/sec. Examination of statistical errors from this fitting procedure gives the interpreter a feel for the consistency of the data and general location of the local seismicity.

A general upper crustal velocity model for the Dixie Valley prospect has been investigated by several authors (Meister, 1967; Eaton, 1963; Hill and Pakiser, 1967). A composite velocity model is shown in Figure 9. Also shown in

Figure 9 is a linear-increase-of-velocity-with-depth model which approximates the composite model $V=V_0+k_z$:

where $V_0$=2.5 km/sec.
k = 0.60km/sec/ km

This linear velocity model produced good statistical fits and consistent locations for events recorded on six or more stations. Table 3 (on Figure 9) lists the velocity model comparisons at various depths.

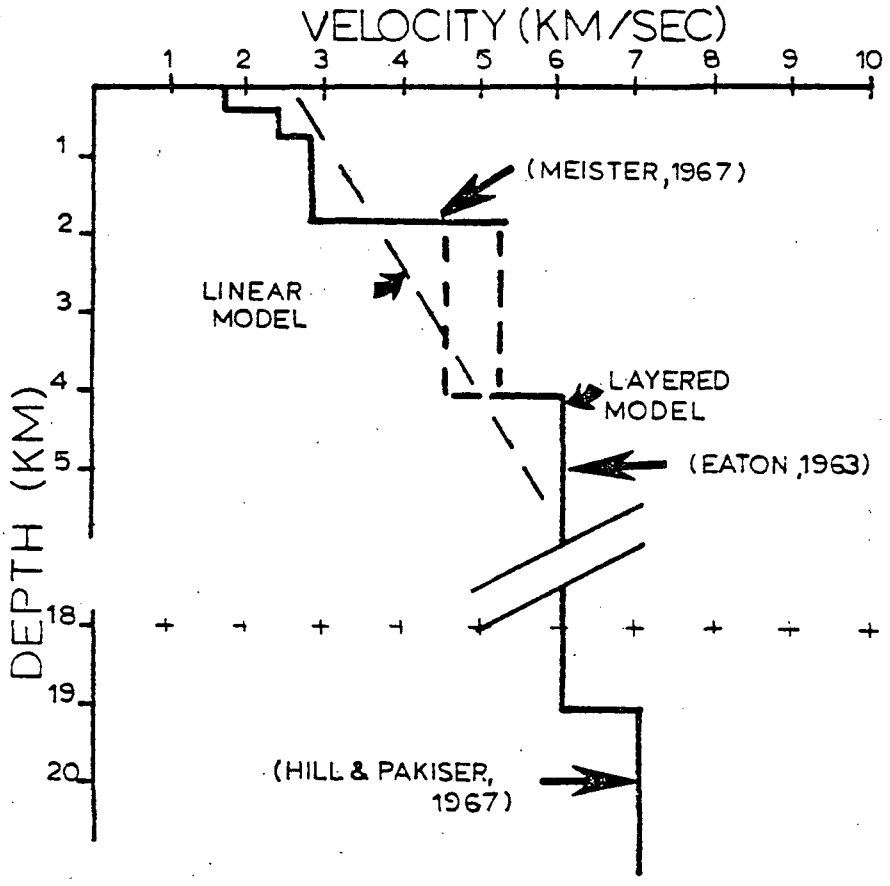


TABLE 3 VELOCITY MODEL

| DEPTH TO TOP OF LAYER (KM) | 0.0 | 2.0 | 4.0 | 19.0 |
|---|---|---|---|---|
| LAYERED MODEL VELOCITY IN LAYER (KM/SEC) | 1.75-2.9 | 4.5-5.3 | 6.0 | 7.0 |
| LINEAR MODEL (KM/SEC) | 2.5 | 3.7 | 4.9 | - |

| | | |
|---|---|---|
| TITLE: VELOCITY MODEL | | |
| SCALE: N/A | APPROVED BY: JRB | DRAWN BY PB |
| DATE: DEC 16, 1976 | | REVISED N/A |
| Micro Geophysics | | DRAWING NUMBER Figure 9 |

## OBSERVATIONS

### Epicenter Locations

Two hundred and sixteen local seismic events were detected during this survey. Of these, 44 were located. The epicenter map on Figure 10 indicates most of the epicenters occurred just south of the hot springs. The 172 events not located were assigned a location by use of the S-P time and signature similarity to well placed events. Almost all of these events occur in the area south of the hot springs. Of the events that were detected within 2 km of the prospect, 90% were located. Therefore no significant seismic information with respect to the prospect area has been omitted.

The hypocenter map reproduced at a scale of 1:62500 is in the cover leaf of this report. All the located events are shown with time and depth. A listing of all located events is found in the appendix.

### Time of Occurrence

The number of events-by-date (Figure 11) shows an average of above 11 events occurred per day, with increases of activity on days 298, 302 and 309.

The number-of-events-by-hour-of-occurrence curve (Figure 11) can indicate if the seismicity recorded is man made (by having

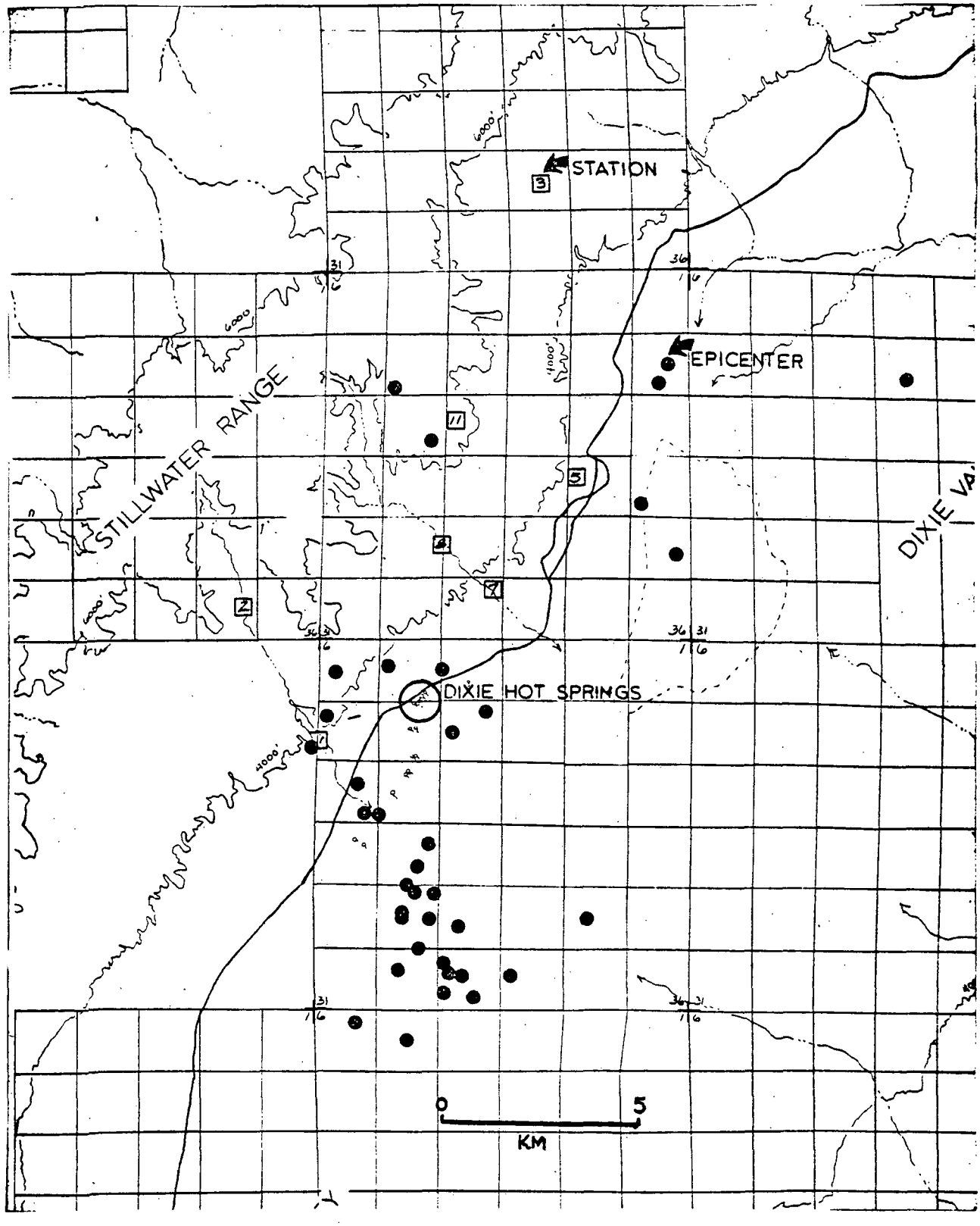


| | | |
|---|---|---|
| TITLE: EPICENTER MAP | | |
| SCALE: N/A | APPROVED BY: JRB | DRAWN BY PB |
| DATE: DEC 18, 1976 | | REVISED N/A |
| Micro Geophysics | | DRAWING NUMBER Figure 10 |

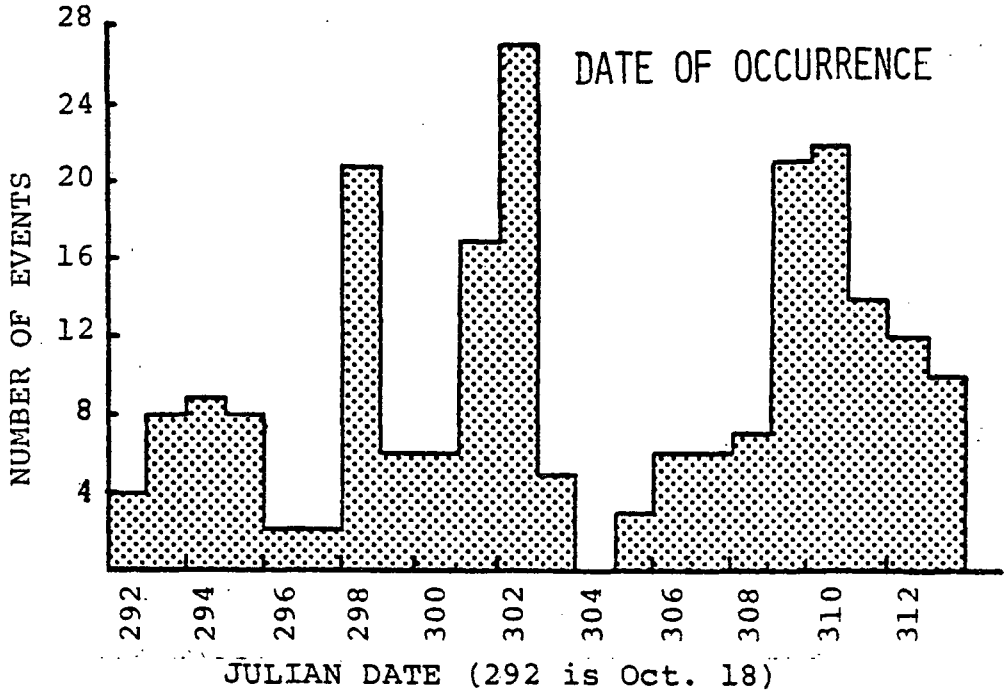


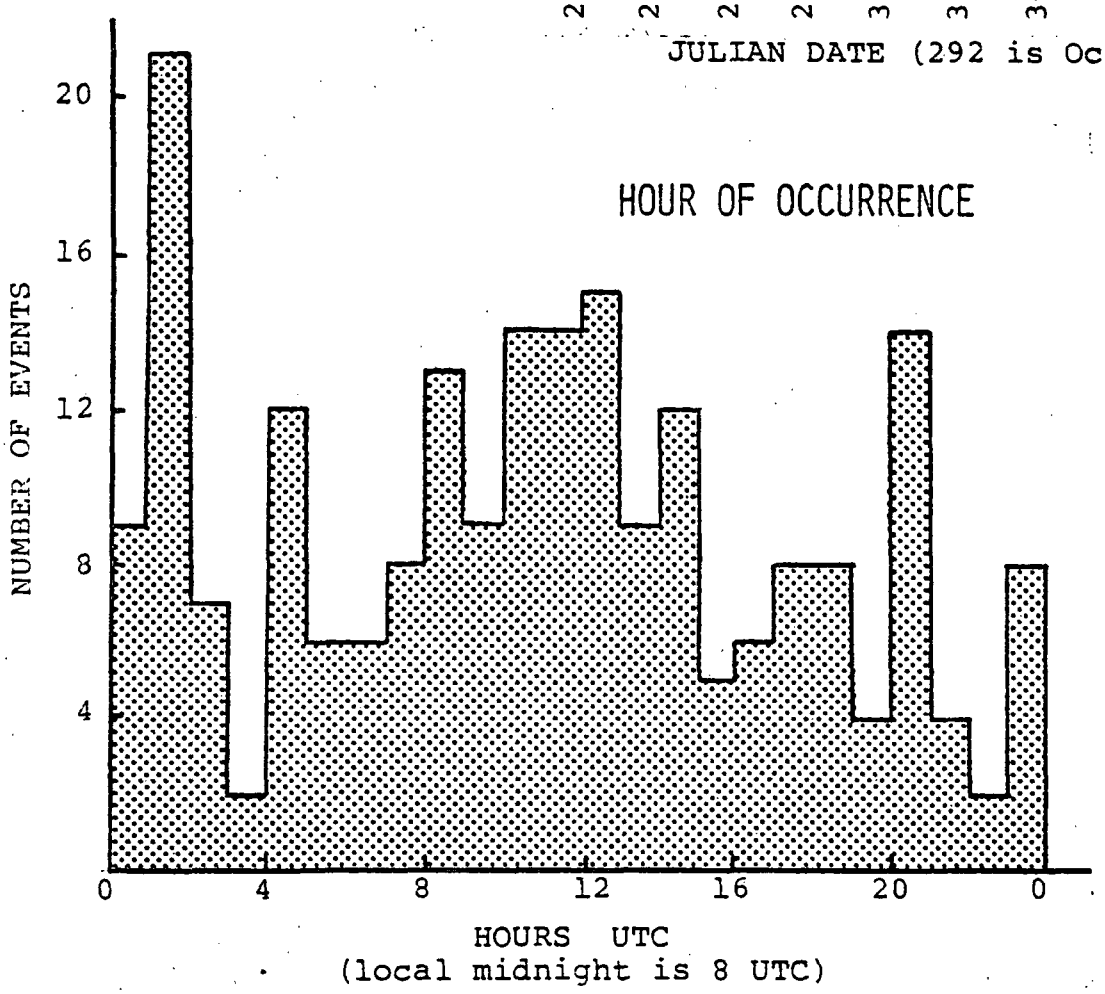


| | | |
|---|---|---|
| TITLE: OCCURRENCE STATISTICS | | |
| SCALE: N/A | APPROVED BY: PLB | DRAWN BY JRB |
| DATE: DEC. 14 | | REVISED N/A |
| Micro Geophysics | | DRAWING NUMBER Figure 11 |

obvious peaks between 8 a.m. and 5 p.m. local time (1600 UTC and 0100 UTC), or if the afternoon cultural and meteorological noise is covering some events (by having an obvious low from 2 p.m. to 7 p.m. local time, 2200 UTC to 0300 UTC).

The graph of hour of occurrence shows no pattern indicating that either local mining activity (explosives) or meteorological causes affected the recording of the local microearthquakes.

Because nearly all events were well-recorded on station #2, the amplitudes of the p-wave on station 2 was used to calculate the magnitude. Using the station 2 amplitudes and the distance from Station 2 to the hypocenter a calculation of the magnitude can be made using curves developed by Brune and Allen (1969).

The magnitudes calculated were then used to construct the recurrence curve of Figure 12. A reference line with a slope of -0.9 is shown on the data and fits fairly well. A b-slope of -0.9 has been determined to be applicable to the Basin and Range (Everdon, 1970).

First Motion Plots and Cross-Section Plots

The first-motion plots are shown in Figures 13 and 14. The first motion of each earthquake is plotted on an upper-hemisphere stereo plot centered at the located hypocenter.

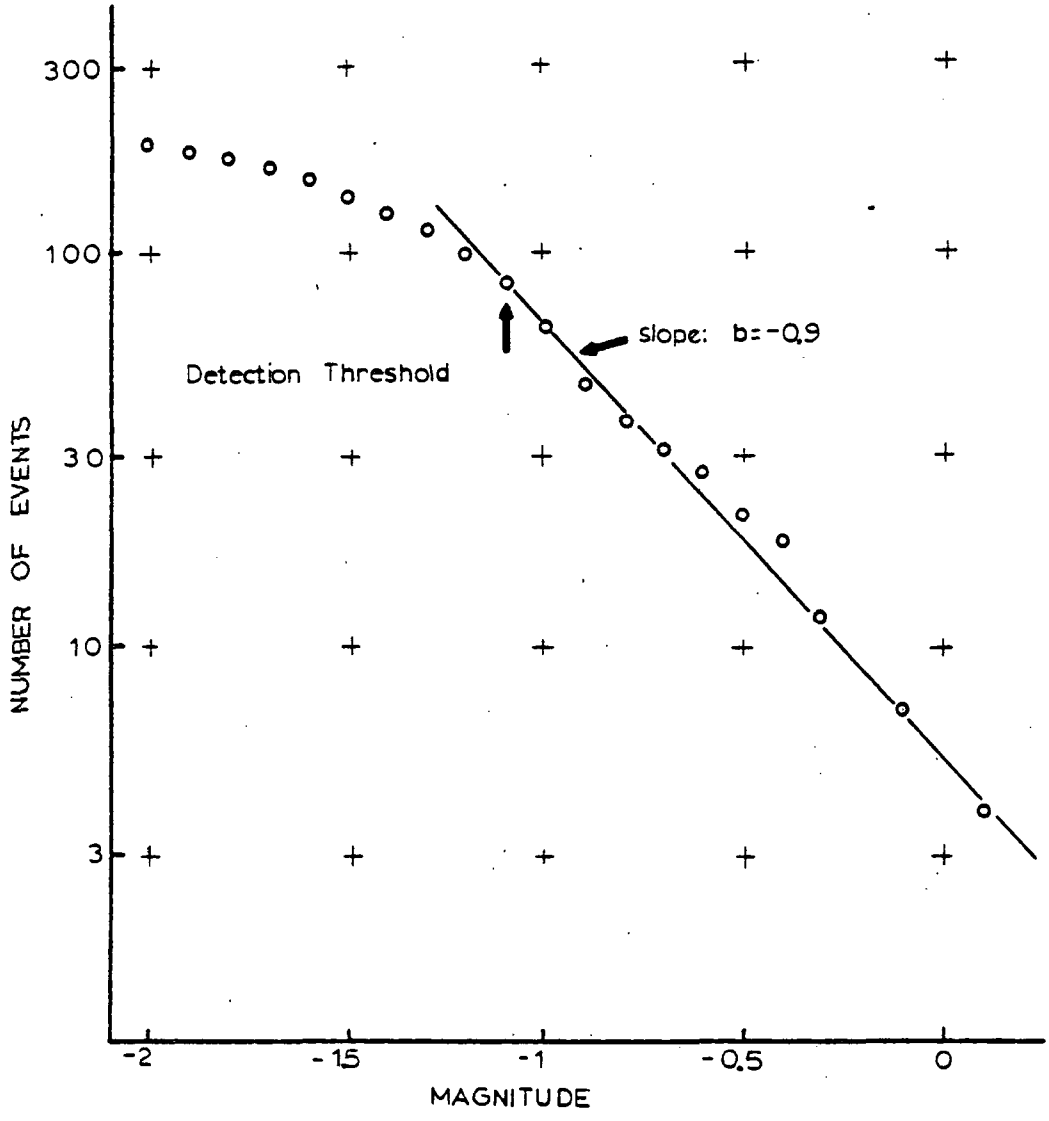


| | | |
|---|---|---|
| TITLE: CUMULATIVE RECURRENCE CURVE | | |
| SCALE: N/A | APPROVED BY: PLB | DRAWN BY JRB |
| DATE: DEC. 16, 1976 | | REVISED N/A |
| Micro Geophysics | | DRAWING NUMBER Figure 12 |

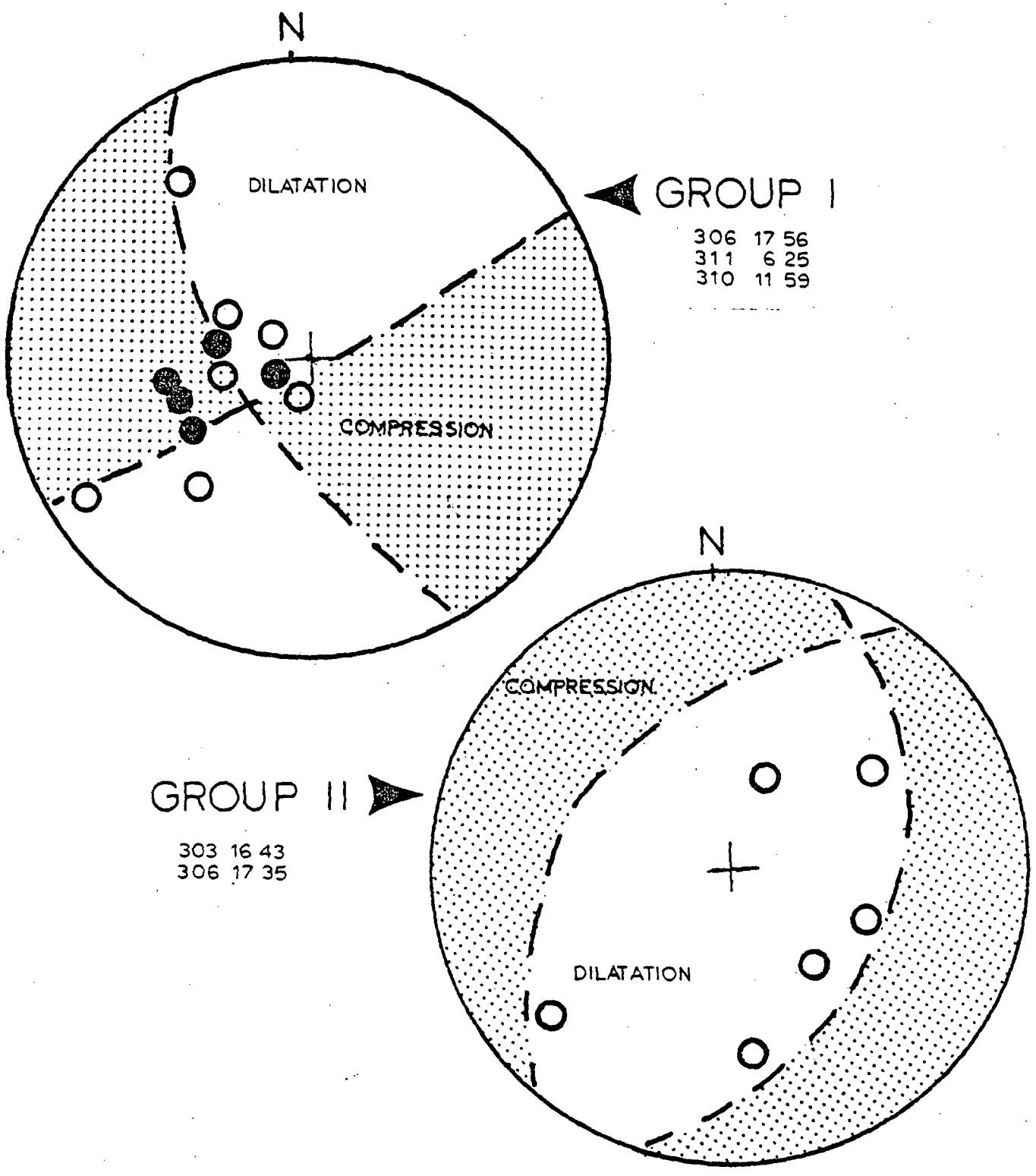


| | | |
|---|---|---|
| TITLE: FIRST MOTION: AREAS I & II | | |
| SCALE: N/A | APPROVED BY: JRB | DRAWN BY PB |
| DATE: DEC. 18, 1976 | | REVISED |
| Micro Geophysics | | DRAWING NUMBER Figure 13 |

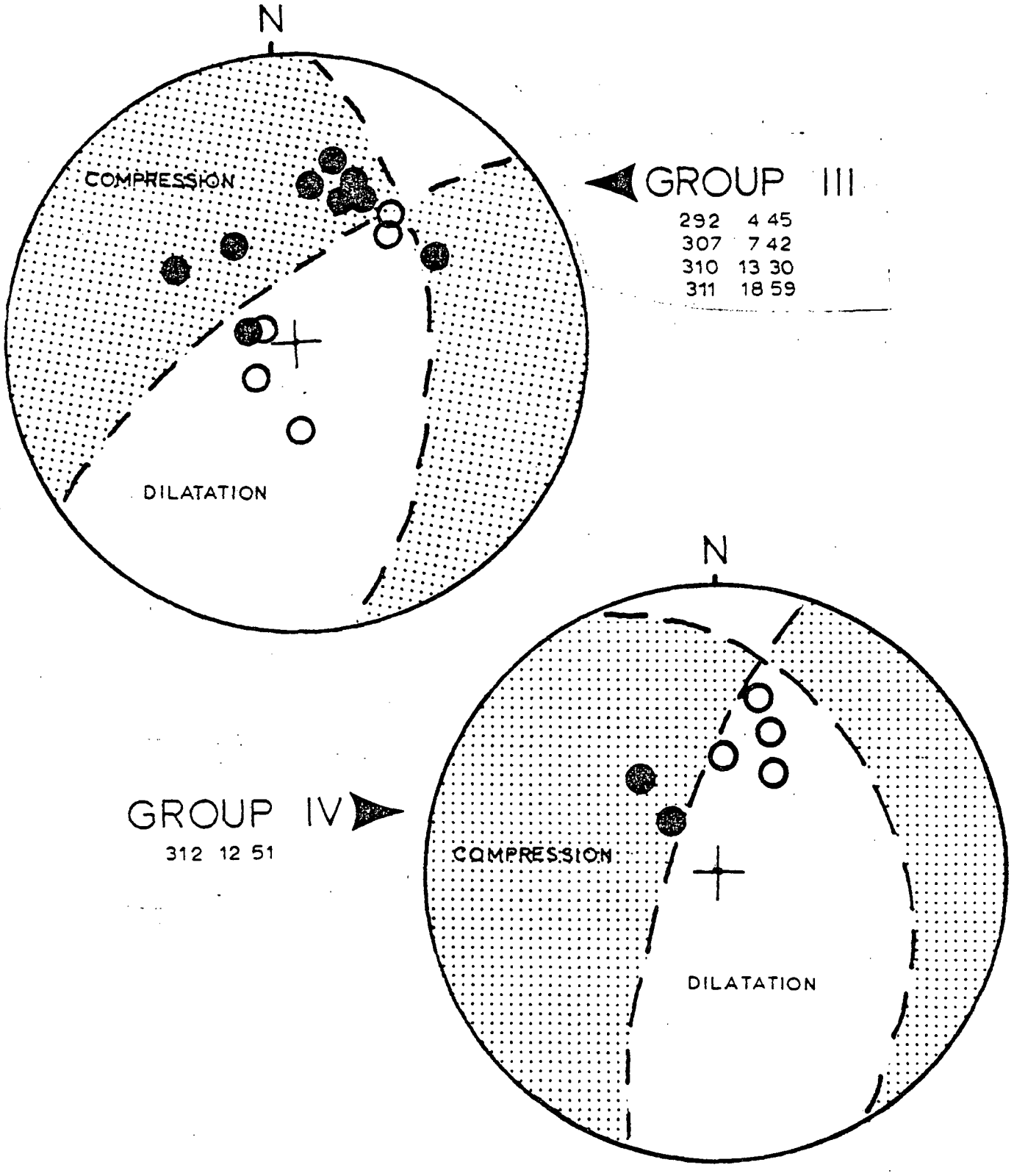


| | | |
|---|---|---|
| TITLE: FIRST MOTION: AREAS III & IV | | |
| SCALE: N/A | APPROVED BY: JRB | DRAWN BY PB |
| DATE: DEC. 18,1976 | | REVISED N/A |
| Micro Geophysics | | DRAWING NUMBER Figure 14 |

The azimuth is the earthquake-to-station azimuth and the angle measured from the vertical corresponds to the take-off angle of the ray which first reaches the station. Thus these plots are highly dependent on the velocity model assumed as both the hypocenter location (particularly the depth) will change if the velocity model is changed as will the take-off angle from the earthquake to the station.

The plots in Figures 13 and 14 will be discussed in order from north to south but the selection of actual fault-plane will be left for the interpretation section. The two most northwesterly events are located within the Stillwater Range. The first motion plots are consistent with northeast-striking normal fault planes but the strike is poorly constrained ($\pm$ 25°). The dip of these two planes is unknown.

Moving southeastward, the picture is better, but the events are also small and to one side of the network (see above signal-to-noise considerations). The three events composited together have first motion plots consistent with two planes: a N 25° W striking, deeply northeast dipping plane and a N 45° E plane with a near vertical attitude. These planes indicate either right-lateral strike-slip motion on the first plane or left-lateral strike-slip with some dip slip motion on the second. The selection of a fault plane is a matter to be interpreted, but the uncertainty in the solutions ($\pm$ 20°) should be borne in mind as the interpretation is reviewed by the reader.

The next group of earthquakes is near and in the vicinity of Station 1. First motions define two planes rather well: a roughly N-S plane with 30-40° of west dip and a northeast plane with very steep dip to the southeast. Selection of one of these planes will be difficult as the first agrees with the general trend of the epicenters but the second is subparallel with the topography and mapped faults in the area. Discussion is deferred to the section on interpretation.

The first motions due to the group of events south of the Dixie Hot Springs are composited on the last stereo plot. Due to the array geometry, these events (which were outside the prospect) have relatively few points on the first-motion plot. Two planes are shown on this plot: a N 30° W plane with 30-40° of southwest dip and a N 20° E striking plane with a steep dip to the southeast. These planes, though poorly constrained, again are consistent with either the strike of the epicenter pattern or the tectonic style of the area.

To utilize the hypocentral data, cross sections were plotted along certain azimuths of interest. Ellipses were plotted on the cross-sections to emphasize the lower accuracy of the depth figure assigned to each hypocenter. The locations of the cross sections are shown on Figure 15.

The first cross section (Figure 16) illustrates that

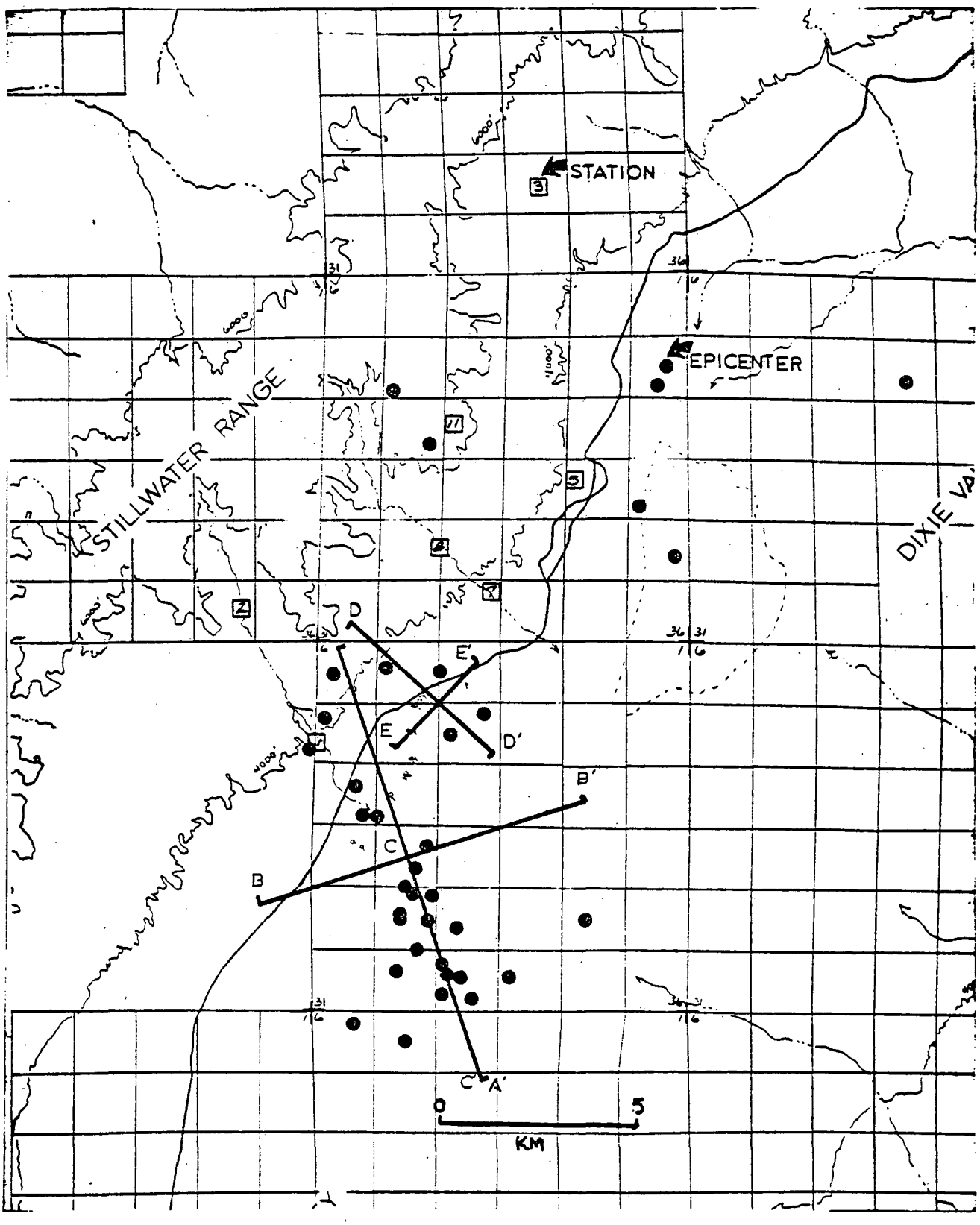


TITLE: CROSSECTION LOCATION MAP

| | | |
|---|---|---|
| SCALE: N/A | APPROVED BY: JRB | DRAWN BY PB |
| DATE: DEC 18, 1976 | | REVISED N/A |
| Micro Geophysics | | DRAWING NUMBER Figure 15 |

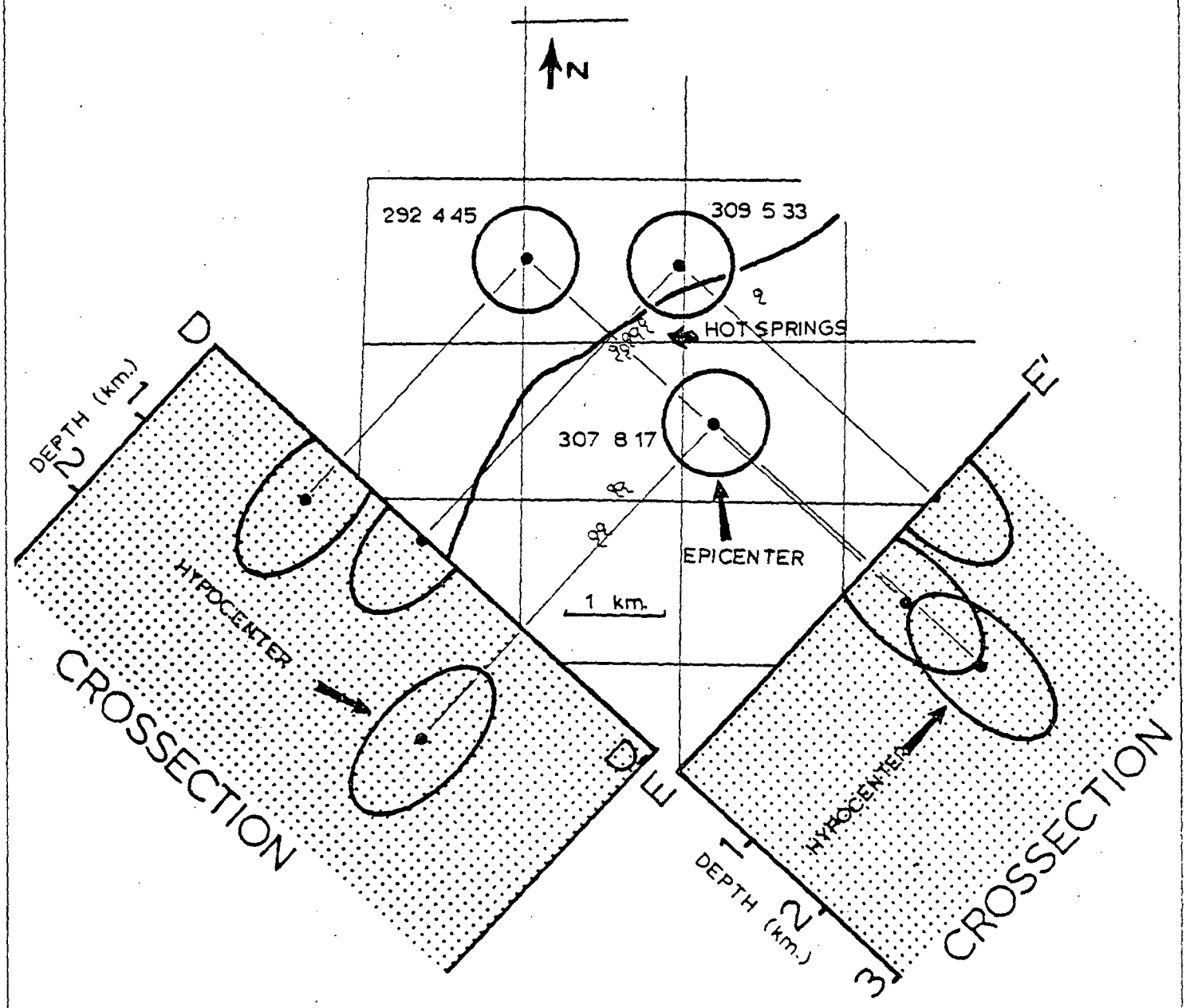


| | | |
|---|---|---|
| TITLE: CROSSECTIONS D-D' & E-E' | | |
| SCALE: N/A | APPROVED BY: JRB | DRAWN BY PB |
| DATE: DEC. 18, 1976 | | REVISED |
| Micro Geophysics | | DRAWING NUMBER Figure 16 |

the faulting near the north end of the hot springs is shallow (less than 3 km). Figure 17 is an easterly view of shallow events selected from the large group of events to the south of the Dixie Hot Springs. These events seem to line up on a east-north east fault-zone with about 45° of dip to the south. The remainder of the cluster south of the hot springs is found beneath the events on Figure 17. These deeper events are plotted on two cross-sectional views on Figure 18. These two cross-sectional views at right angles indicate that the deeper events are consistent with a steeply dipping, NW trending fault or a more moderately dipping, NE trending fault (to within the precision of the locations).

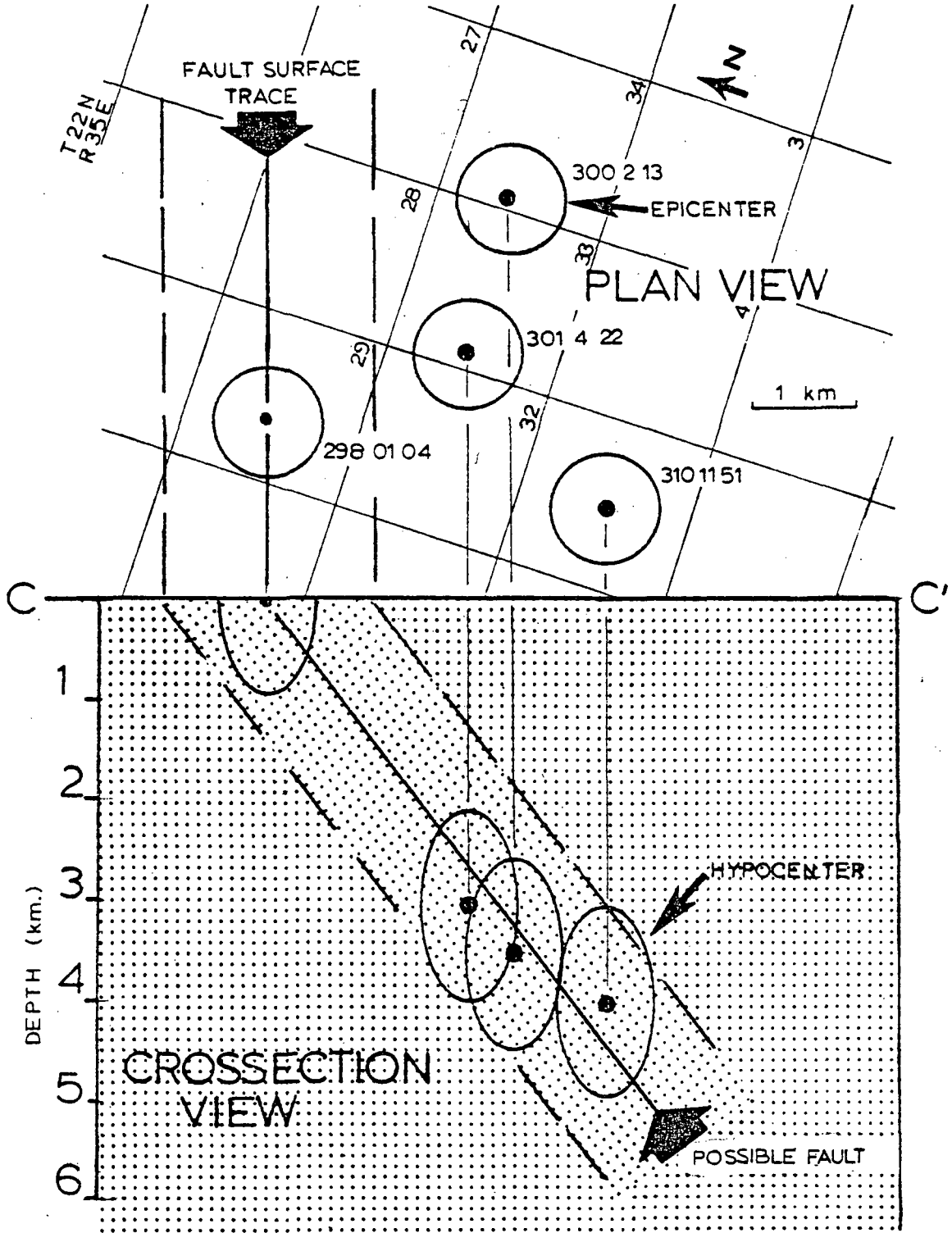


| | | |
|---|---|---|
| TITLE: CROSSECTION C-C' | | |
| SCALE: N/A | APPROVED BY: JRB | DRAWN BY PB |
| DATE: DEC. 18, 1976 | | REVISED N/A |
| Micro Geophysics | | DRAWING NUMBER Figure 17 |

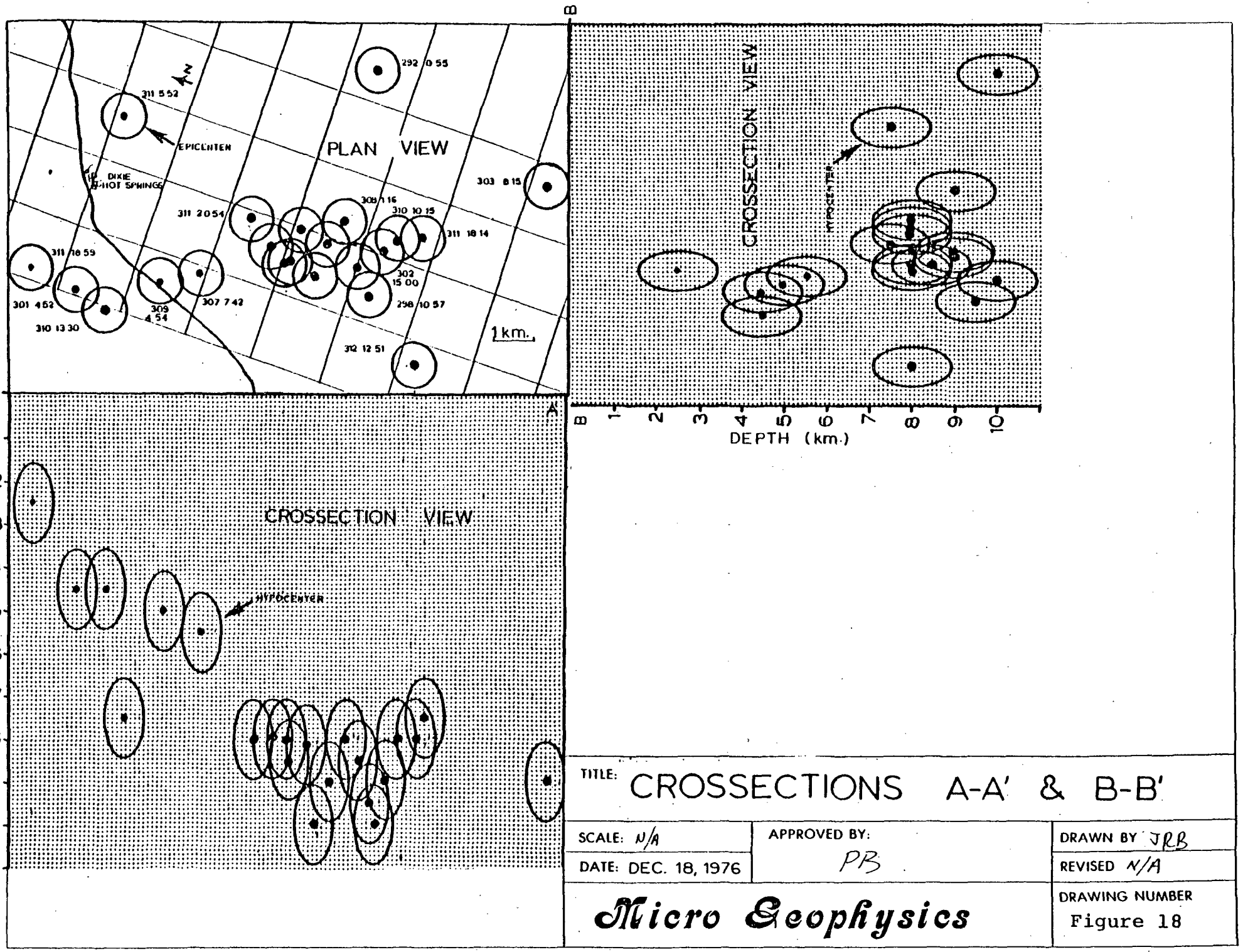


TITLE: CROSSECTIONS A-A' & B-B'

| | | |
|---|---|---|
| SCALE: N/A | APPROVED BY: PB | DRAWN BY JRB |
| DATE: DEC. 18, 1976 | | REVISED N/A |
| Micro Geophysics | | DRAWING NUMBER Figure 18 |

## INTERPRETATION

The interpretation, as distinguished from the observations above, will focus on the prospect area. The active seismic patterns to the south will be reviewed and then the similar but less conclusive data on the prospect will be interpreted from the viewpoint of homogeneity of tectonic style from south to north. Due to the historical macroseismic activity in the area, care must be exercised in equating seismicity with geothermal activity. The fault-plane solutions, due to the ambiguity problem, have no unique interpretation. The favored interpretation of the seismicity is, however, consistent with the geological patterns observed both south and north of the prospect area.

The historical seismicity (Figure 3) indicates an aseismic gap in the prospect area. The fault model of Ryall and Malone (1971) (Figure 4) indicates long oblique-slip NNW-trending segments (with significant strike-slip components) connected by short NE-trending dip-slip segments. The preferred interpretation of the cluster of events south of the hot springs is that they are part of one of the NW-trending oblique slip zones. Near where this zone intersects the highway, the events are interpreted to lie on a NE-trending dip-slip zone. This zone trends into the prospect area and

is intersected by another oblique-slip zone which has a NNW-trend.

A persuasive point for this interpretation is the fact that the NE trending normal fault zone is subparallel and spatially close to the geologically mapped boundary fault of the Stillwater range.

Two events high up in the Stillwater range are almost certainly on a NE-trending dip-slip zone that is down towards the valley.

An alternative interpretation of all seismicity recorded off the prospect is NE-trending en echelon normal faults down to the valley. However on the prospect the fault-plane solution requires and constrains a strike-slip mechanism. The mechanisms are either a right-lateral, N 20° W striking, fault or a left-lateral, NE-striking fault. The important conclusions is that in or near the prospect the mechanism of faulting changes and fault intersections are present in the prospect area.

The group of events south of the hot springs is in a historical swarm zone. A swarm is defined as a large number of events concurrent in space and time. The events recorded during this survey are consistent with this background. To illustrate this observation, a qualitative strain-release map was prepared as Figure 19. Events to the north are enclosed by a dotted contour as all events detected are present on this map. The southern group

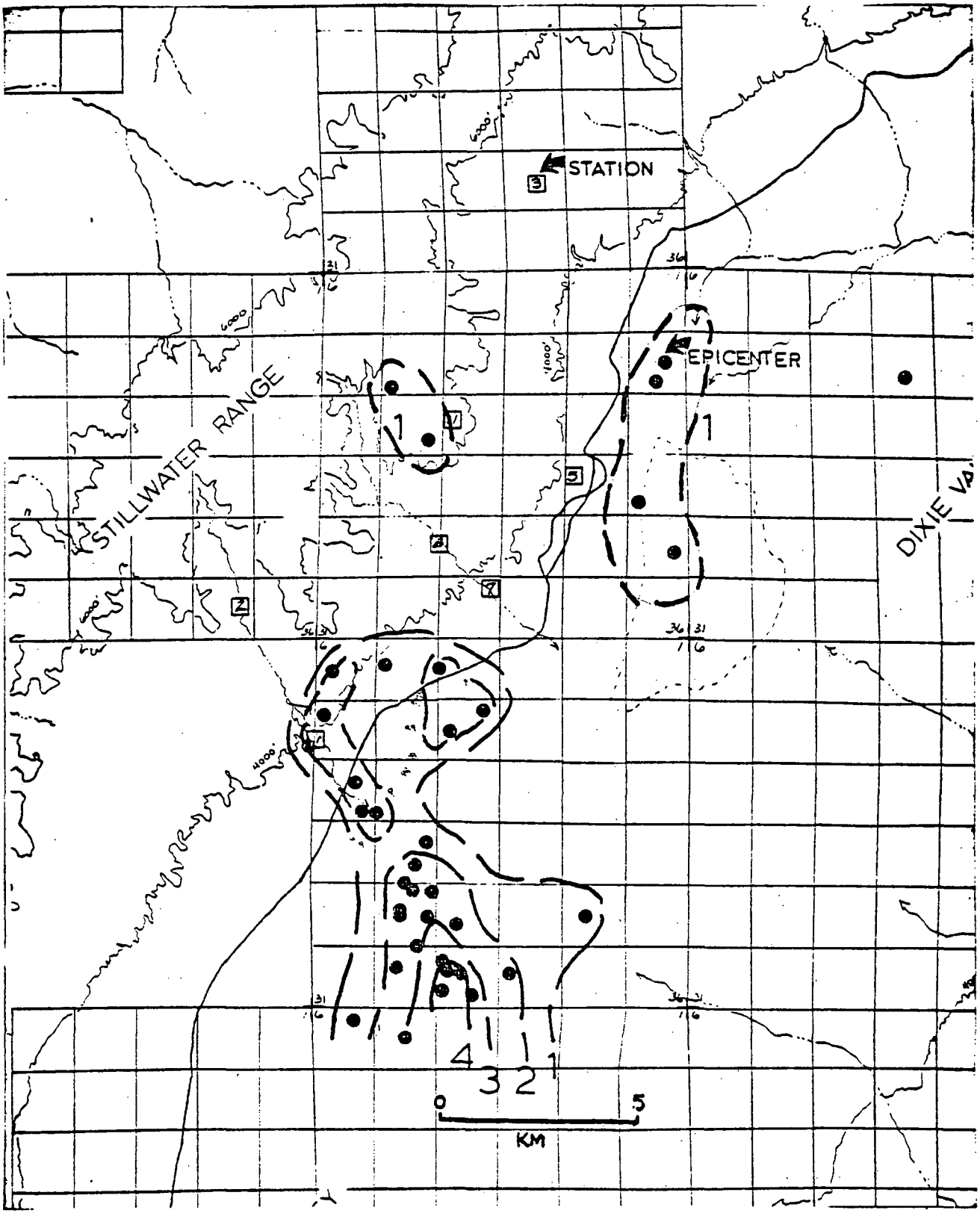


Contour values represent relative strain release.

TITLE: QUALITATIVE STRAIN RELEASE

| | | |
|---|---|---|
| SCALE: N/A | APPROVED BY: JRB | DRAWN BY PB |
| DATE: DEC 18, 1976 | | REVISED N/A |
| Micro Geophysics | | DRAWING NUMBER Figure 19 |

has numerous contours as many small events were detected in the swarm zone south of the hot springs. Figure 20 is a schematic diagram delineating the nature of the regional tectonics from south to north. The northeast striking faults in Figure 20 are interpreted to be oblique slip, the northwest striking fault, dip-slip. Figure 21 indicates the volume of seismicity near station 2. Note that the scale is logarithmic; the majority of these events are 10-12 km from station 2, i.e. south of the Dixie Hot Springs.

The seismicity rate in the immediate vicinity of the prospect is not high, near one event per 3-5 days. However, with respect to seismic risk, the important point is the extension of the tectonic style from the Fairview Peak-Dixie Valley part of the Nevada Seismic zone northward past the prospect. Such an extension has been previously proposed on geologic grounds, but the microearthquake evidence from this survey definitely indicates that such an extension is likely. The implications of this extension are in the area of seismic risk to wells or other structures built on this zone. A pessimistic view would be that events as large as the Fairview Peak-Dixie Valley earthquake (Richter magnitude 6.8!) could happen within the prospect area. Careful economic analysis, return-time estimates, and ground-acceleration maps should be prepared if commercial development of the geothermal resources is contemplated.

This interpretation has indicated the likelihood of active fault intersections within the prospect area, a moderate but important seismicity rate, and an extension of the regional tectonics of a major seismic zone south of the prospect area.

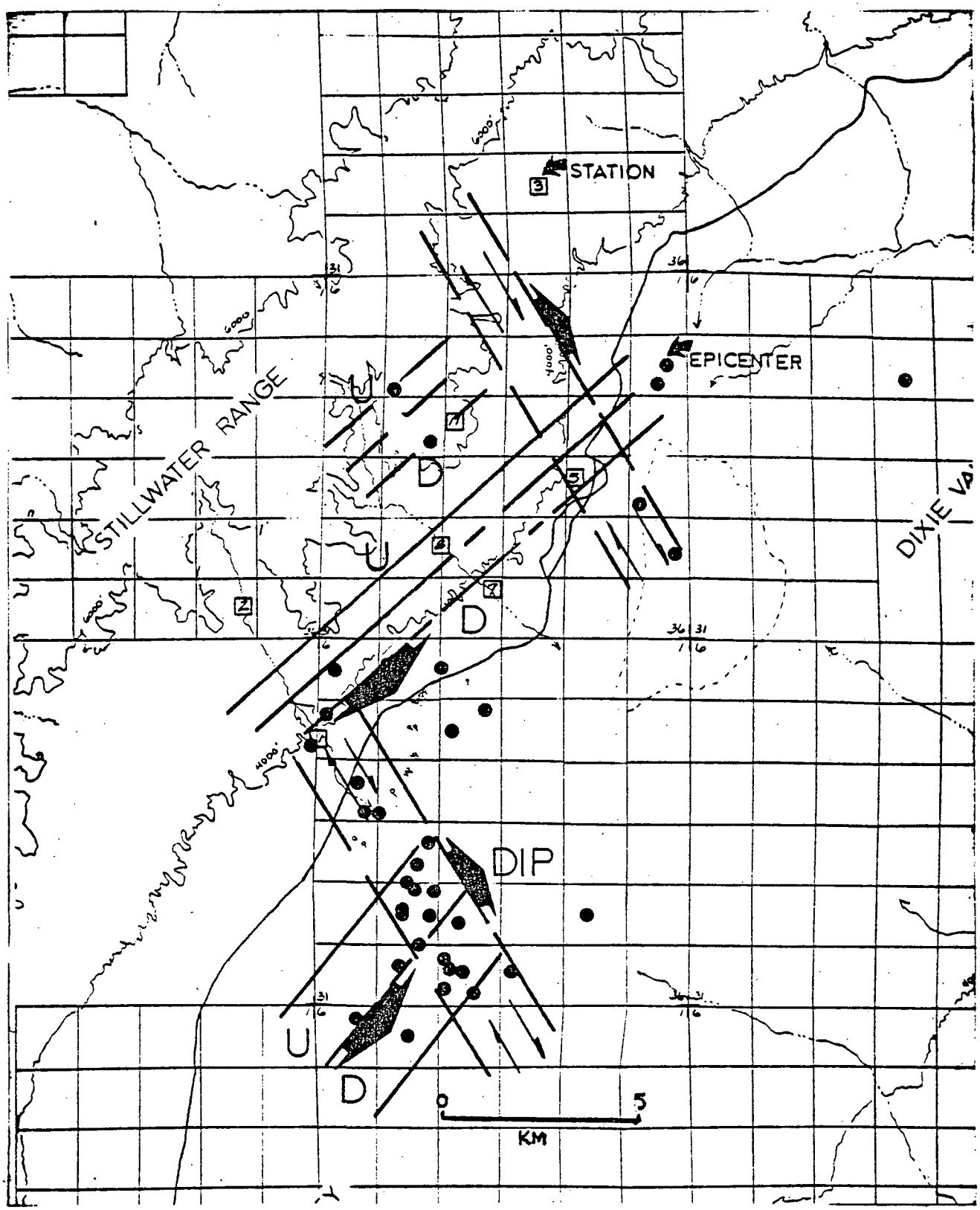


TITLE: REGIONAL TECTONICS

| | | |
|---|---|---|
| SCALE: N/A | APPROVED BY: JRB | DRAWN BY PB |
| DATE: DEC 18, 1976 | | REVISED N/A |
| Micro Geophysics | | DRAWING NUMBER Figure 20 |

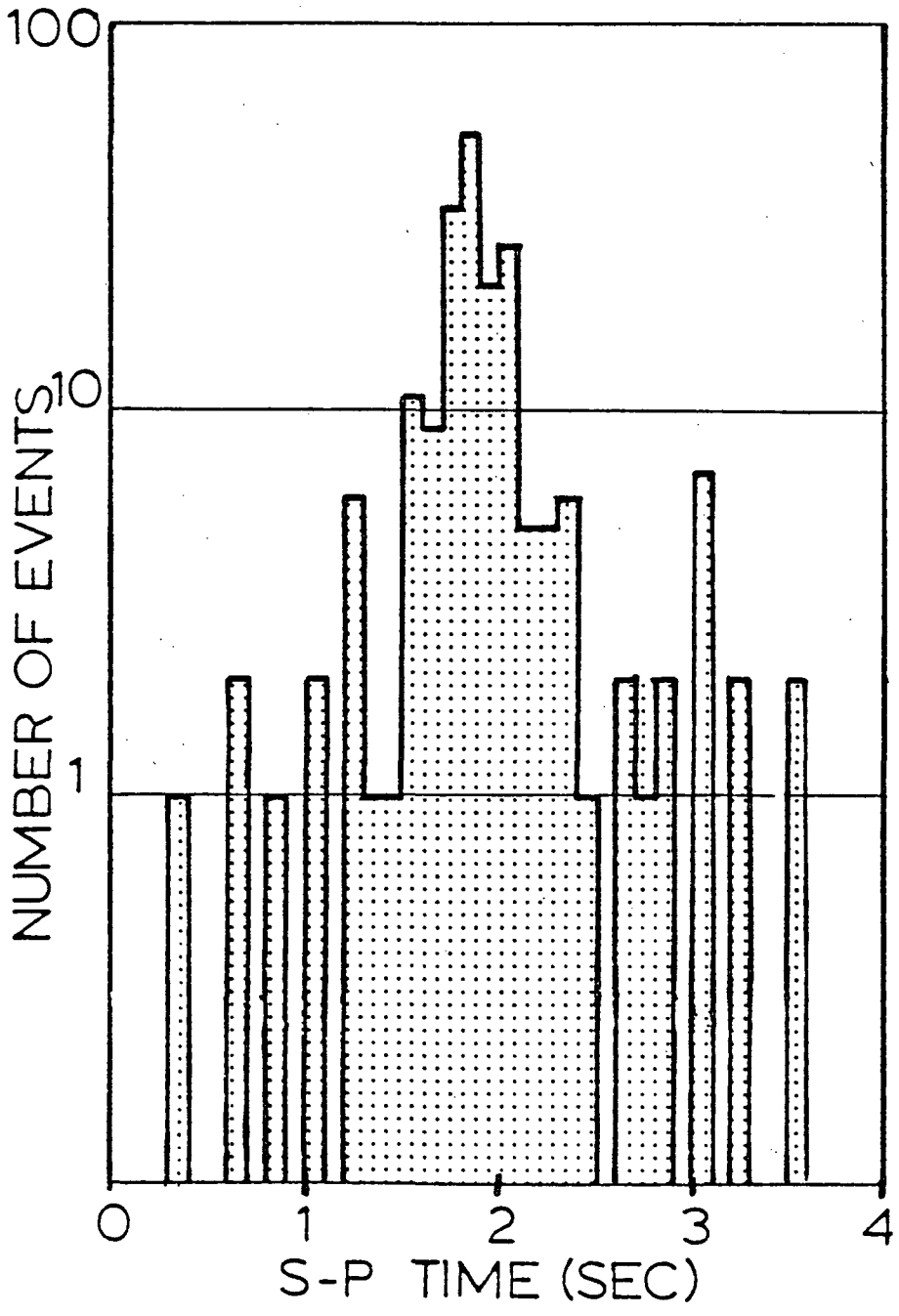


| | | |
|---|---|---|
| TITLE: S-P TIME FROM STATION 2 | | |
| SCALE: DEC. 18,1976 | APPROVED BY: JRB | DRAWN BY PB |
| DATE: N/A | | REVISED N/A |
| Micro Geophysics | | DRAWING NUMBER Figure 21 |

## CONCLUSIONS

1. Seismically active faults are present in the prospect area. First-motion studies indicate fault intersections that are seismically favorable areas for the occurrence of earth steam are present near station 5 on the prospect area.

2. Upon confirmation of a heat source and a favorable groundwater regime, the prospect should be tested for commercial production of geothermal resources.

3. The seismic risk in this area is high. This survey confirms the extension of the Nevada Seismic Zone across the prospect area.

## RECOMMENDATIONS

1. The existence of a heat source and a favorable water supply situation should be confirmed by electrical resistivity and hydrologic studies.
2. Upon confirmation of a favorable geologic environment and from the seismological point of view, this area is an excellent geothermal prospect.
3. When commercial exploitation is begun, seismic activity associated with the withdrawal and injection of fluids must be carefully monitored in order to isolate any adverse environmental effects.
4. This area is subject to substantial seismic risk. Construction in the area must conform to adequate building codes in order to minimize the probable earthquake risk.

## REFERENCES


Brune, James and Clarence Allen, 1967, A microearthquake survey of the San Andreas fault system in Southern California, BSSA, vol. 57, no. 2, p. 277.

Chinnery, Michael A., 1969, Earthquake Magnitude and Source Parameters, BSSA, vol. 59, no. 5, p. 1969.

Douglas, B. M. and Ryall, A., 1972, Spectral Characteristics and stress drop for microearthquakes near Fairview Peak, Nevada, JGR, vol. 77, no. 2, p. 351.

Evernden, J. F., 1970, Study of Regional Seismicity and Associated Problems, BSSA, vol. 60, no. 2, p. 393.

Gumper, F. J., and Scholz, C., 1971 Microseismicity and tectonics of the Nevada seismic zone, BSSA, vol. 61, no. 5, p. 1413.

Hamilton, R. M. and L. J. P. Muffler, 1972, Microearthquakes at the Geysers Geothermal area, California, JGR, vol. 77, no. 11, p. 2081.

Herring, A. T., 1967, Seismic refraction study of a fault zone in Dixie Valley, Nevada, A. F. Cambridge Research Labs Final Scientific Report Part II, AFCRL - 66-848.

Lange, A. L. and W. H. Westphal, 1969, Microearthquakes near the Geysers, Sonoma County, California, JGR, vol. 74, p. 4377.

Meisler, L. J., 1967, Seismic refraction study of Dixie Valley, Nevada, A. F. Cambridge Research Labs Final Scientific Report Part I, AFCRL-66-848.

Meister, L. J., Buford, R. O., Thomson, G. A. and R. C. Kovach, 1968, Surface-strain changes and strain energy release in the Dixie Valley-Fairview Peak area, Nevada, JGR, vol. 73, no. 18, p. 5981.

Peters, David and Robert Crosson, 1972, Application of prediction analysis to hypocenter determination using a local array, BSSA, vol. 62, no. 3., p. 775.

Romney, C., 1957, Seismic waves from the Dixie Valley-Fairview Peak earthquakes, BSSA, vol. 47, no. 4, p. 301.

Ryall, A., 1970, 1971, Bulletin of the Seismological Laboratory, Mackay School of Mines.

Ryall, A. and Mallone, S. D., 1971, Earthquake distribution and mechanism of faulting in the Rainbow Mountain-Dixie Valley-Fairview Peak area, central Nevada, JGR, vol. 46, no. 29, p. 7241.

Slemmons, D. B., 1957, The Dixie Valley-Fairview Peak, Nevada, earthquakes of December 16, 1954: geologic effects, BSSA, vol. 47, no. 4, p. 353.

Stauder, W. and Ryall, A., 1967, Spatial distribution and source mechanism of earthquakes in central Nevada, BSSA, vol. 57, no. 6, p. 1317.

Ward, P. L., 1972, Microearthquakes: Prospecting tool and possible hazard in the development of Geothermal Resources, Geothermics, vol. 1, no. 1, p. 3.

Ward, P. L. and S. Bjornson, 1971, Microearthquakes, Swarms and Geothermal areas of Iceland, JGR, vol. 76, no. 17, p. 3953.

Ward, P. L. and R. H. Jacob, 1971, Microearthquakes: In the 'Anuachapan Geothermal Field, El Salvador Central America, Science, vol. 173, p. 328.

Westphal, W. H. and Lange, A. L., 1967, Local seismic monitoring Fairview Peak area, Nevada, BSSA, vol. 57, no. 6, p. 1279.

APPENDIX

INSTRUMENTATION

The microearthquake network, used for geothermal exploration and deployed by MicroGeophysics Corporation, consists of from six to eight independent microearthquake recording systems. Each system contains an L-4-C vertical seismometer, a MEQ-800-B visual drum recorder with an integral timing system synchronized to universal coordinated time (U.T.C.). Figure 1 is a schematic of the microearthquake recording system. A detailed explanation of the component parts is given below.

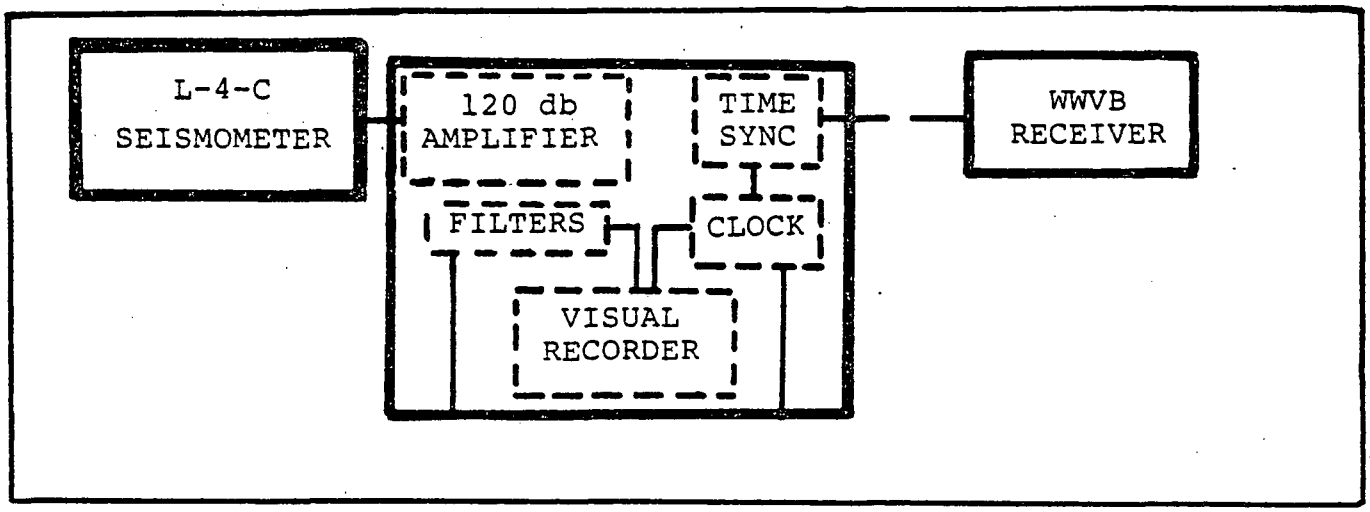


Figure 1

L-4-C

The L-4-C is a one-hertz-natural-frequency vertical seismometer. The damping is 0.6 of critical damping. The L-4-C has an output of 6.9 volts per inch/second.

Geophones are planted on solid rock in protected locations consistent with the geometrical requirements of appropriate array shape and access considerations. The field monitor allows a rapid evaluation

of each geophone plant over a 24 hour period and poor stations (noisy, bad earthquake signatures, low gain) are immediately moved to favorable sites.

## MEQ-800-B

The MEQ-800-B is a visual microearthquake recorder. The smoked drum recording has a nominal 120mm/min rotation speed with 1mm spacing between succeeding traces. The stylus and trace width is 0.05mm. The amplifier has a maximum of 120db of gain and selectable high and low cut filters. The low cut filter has selectable corners at 1, 5 and 10 Hz. The high cut filter has selectable corners at 10, 20, and 75 Hz. The amplifier gains can be changed by precise 6db steps down from 120db. The maximum pen deflection is $\pm$25mm and can be limited under severe ground noise conditions to $\pm$10mm or $\pm$5mm.

The integral timing system consists of a clock, whose drift rate is less than $\pm$1 part in $10^7$ (approximately $\pm$10ms per day) and can be set to standard time and adjusted at 16ms increments. Time is displayed on each trace by a slight deflection of the pen each second.

The frequency characteristics of the instrument are summarized in Figure 2I. Both the velocity and displacement response for the MEQ-800-B microearthquake system are shown. The displacement response at a particular frequency (f) can be calculated by multiplying the velocity gain at f times 2 f. The filter response and gain level shown are typical settings for operations in the western continental United States.

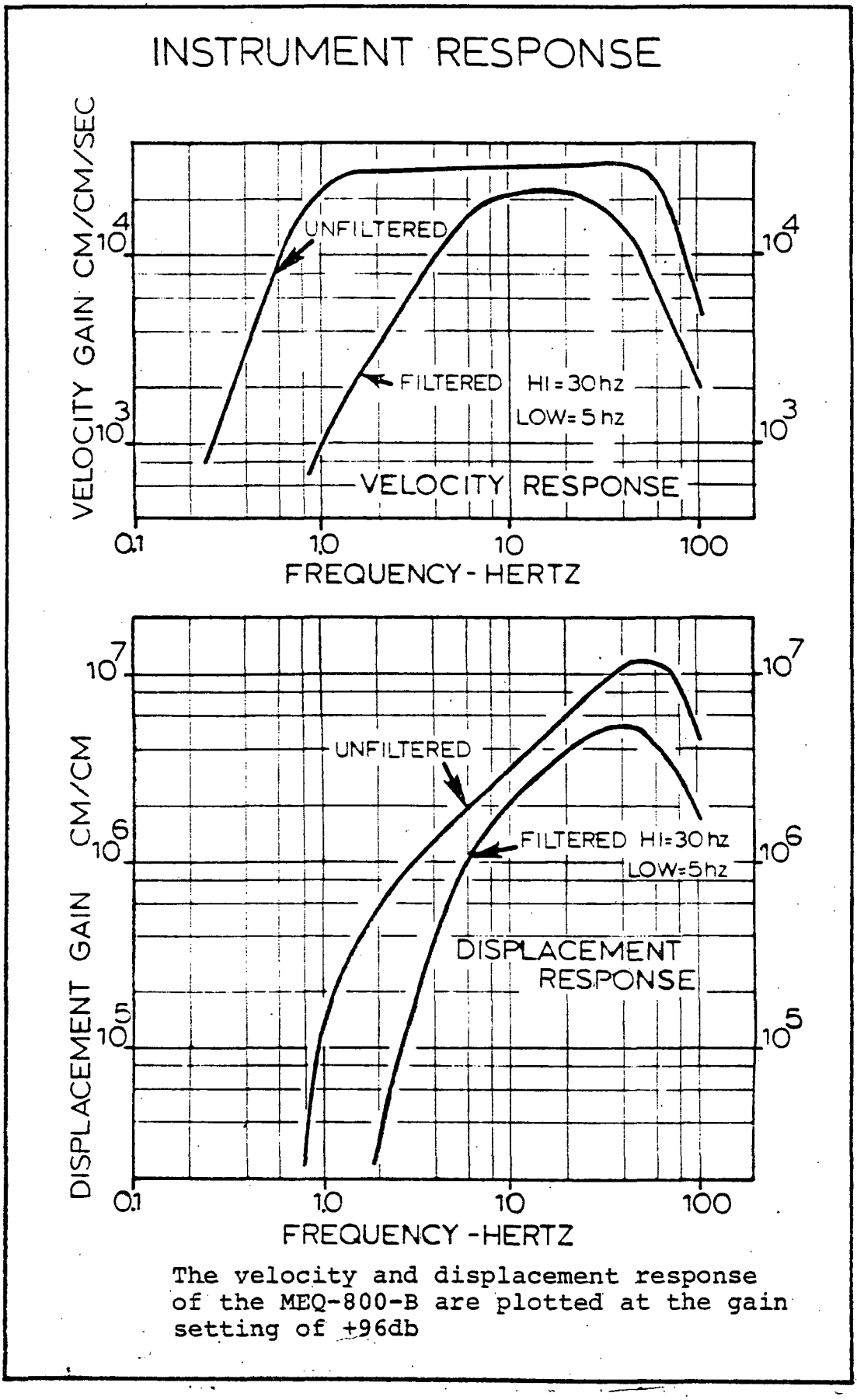
INSTRUMENT RESPONSE
VELOCITY GAIN CM/CM/SEC
UNFILTERED
FILTERED HI=30hz
LOW=5hz
VELOCITY RESPONSE
FREQUENCY-HERTZ
DISPLACEMENT GAIN CM/CM
UNFILTERED
FILTERED HI=30hz
LOW=5hz
DISPLACEMENT RESPONSE
FREQUENCY-HERTZ
The velocity and displacement response of the MEQ-800-B are plotted at the gain setting of +96db

Figure 2I

## WWVB

WWVB is the radio call code for the National Bureau Standards 60khz time-standard station in Fort Collins, Colorado. The WWVB time standard is used to set and synchronize the microearthquake system clocks. As shown in Figure 3A below, the signal consists of 60 markers each 1 minute, with one marker each second. (Time progresses from left to right) each marker is generated by reducing the power of the carrier by 10db at the beginning of the corresponding second and restoring it:

1) 0.2 seconds later for a binary zero
2) 0.5 seconds later for a binary one
3) 0.8 seconds later for a 10 second position marker for a minute reference marker.

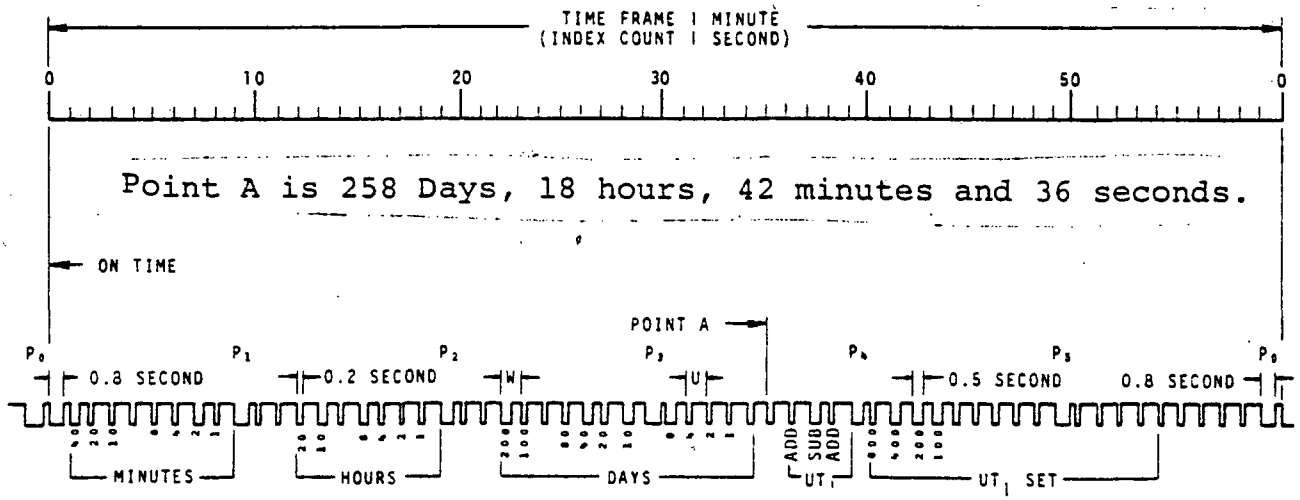


Figure 3

The WWVB code (as shown in Figure 3) is recorded daily on the visual drum as absolute time and date identification of the record, and is used to synchronize each MEQ system to standard time.

The MEQ systems clocks are synchronized daily with WWVB by comparing (on an oscilloscope) the beginning of the WWVB second pulse with the MEQ-800-B internally generated one-second pulse. This comparison can be done to $\pm 2$ milliseconds. Daily records are kept

on the amount of correction for each clock. These time corrections are then applied to the records. Common corrections are on the order of 15ms per day or less than one millisecond per hour.

## DATA

An example of the output of a microearthquake system is shown in Figure 4.

The smoked paper record is used at the time of the recording (in the field) to estimate the seismicity and to locate any recorded microearthquake approximately. The smoked paper records can be picked under magnification to a precision of less than ±30ms. A level of ±30ms timing precision is sufficient to insure that the location uncertainty is almost entirely governed by the inaccuracies in the velocity model (Johnson, 1975).

# EXAMPLE OF A LOCAL EVENT

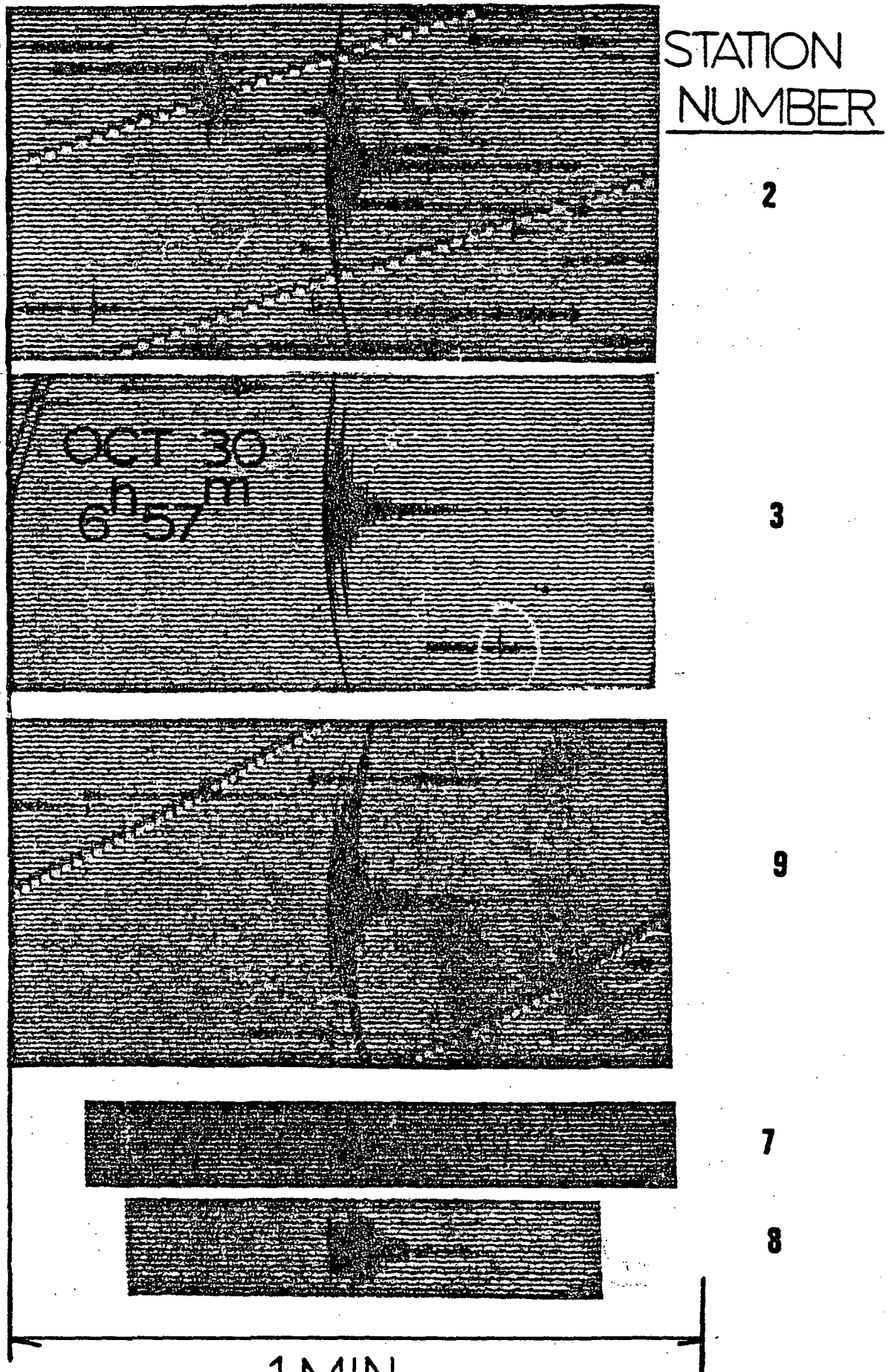


fig 4

## Epicenter Appendix

### Located Events

| Day | Time | X (km) | Y (km) | Z (km) | M |
|---|---|---|---|---|---|
| 292 | 445 | 14.8 | 34.0 | .5 | -0.9 |
| 293 | 055 | 20.5 | 27.5 | 10.0 | 0.1 |
| 293 | 934 | 16.0 | 26.6 | 8.0 | -0.8 |
| 293 | 1059 | 15.5 | 28.4 | 8.5 | -0.6 |
| 293 | 1615 | 15.8 | 28.3 | 8.0 | -0.6 |
| 298 | 104 | 15.6 | 27.5 | 0.0 | -0.8 |
| 298 | 1057 | 15.5 | 26.2 | 9.5 | -0.5 |
| 300 | 213 | 18.0 | 26.0 | 3.5 | -1.9 |
| 301 | 422 | 16.5 | 26.0 | 3.0 | -1.0 |
| 301 | 452 | 13.3 | 32.6 | 4.5 | -2.2 |
| 301 | 1810 | 16.5 | 12.3 | 1.5 | 0.1 |
| 302 | 348 | -5.8 | 55.2 | 22.5 | -1.3 |
| 302 | 1500 | 16.7 | 26.2 | 9.0 | -0.3 |
| 303 | 815 | 19.0 | 22.8 | 9.0 | -1.0 |
| 303 | 1643 | 15.1 | 41.3 | 4.0 | -2.0 |
| 306 | 320 | 4.8 | 21.2 | 0 | 3 |
| 306 | 412 | 16.0 | 28.7 | 8.0 | -1.0 |
| 306 | 1735 | 16.2 | 39.9 | 1.0 | -1.4 |
| 306 | 1756 | 22.2 | 41.3 | 1.0 | -0.4 |
| 307 | 742 | 14.7 | 30.0 | 5.5 | -1.0 |
| 307 | 817 | 16.8 | 32.3 | 1.5 | -1.1 |

 

Epicenter Appendix - Located Events



| Day | Time | X (km) | Y (km) | Z (km) | M |
|---|---|---|---|---|---|
| 308 | 1955 | 14.8 | 30.2 | 4.0 | -1.3 |
| 309 | 116 | 16.8 | 27.1 | 8.0 | -0.5 |
| 309 | 454 | 14 | 30.9 | 5.0 | -1.6 |
| 309 | 533 | 16.5 | 33.9 | 0 | -1.3 |
| 309 | 1657 | -9.2 | 38.7 | 4.5 | -0.3 |
| 310 | 931 | 16.3 | 28.2 | 8.0 | 0.2 |
| 310 | 1015 | 16.9 | 26.0 | 8.0 | -1.0 |
| 310 | 1028 | 16.5 | 25.6 | 8.0 | -0.4 |
| 310 | 1151 | 15.5 | 24.2 | 4.0 | -1.0 |
| 310 | 1159 | 22.6 | 36.8 | 8.0 | -0.9 |
| 310 | 1330 | 13.0 | 31.9 | 4.5 | -1.1 |
| 311 | 552 | 18.7 | 33.0 | 7.5 | -0.6 |
| 311 | 625 | 21.5 | 38.2 | 8.0 | -1.4 |
| 311 | 1814 | 17.0 | 25.3 | 7.5 | -0.6 |
| 311 | 1859 | 13.4 | 33.8 | 2.5 | -1.0 |
| 311 | 2047 | 16.2 | 27.5 | 9.0 | -0.3 |
| 311 | 2054 | 16.2 | 29.5 | 8.0 | -0.1 |
| 312 | 1251 | 14.2 | 24.7 | 8.0 | -0.1 |
| 313 | 240 | 15.3 | 27.5 | 10.0 | -1.6 |
| 313 | 807 | 22.7 | 42.0 | 4.5 | -1.8 |
| 313 | 808 | 29.1 | 41.7 | 5.0 | -2.9 |

Epicenter Appendix - Located Events



| Day | Time | X (km) | Y (km) | Z (km) | M |
|---|---|---|---|---|---|
| 313 | 838 | 13.4 | 18.7 | 0 | 1.0 |
| 313 | 1115 | 21.9 | 52.2 | 7 | 0.3 |

The origin is located at latitude 39°30' N, longitude 118°15' W. Z is the event depth below a datum of 1 km above sea level. Positive X and Y are east and north respectively. M is event magnitude.